Cellular/Molecular

An Alien Divalent Ion Reveals a Major Role for Ca^{2+} Buffering in Controlling Slow Transmitter Release

Norbert Babai,[1] Olexiy Kochubey,[1] Daniel Keller,[2] and Ralf Schneggenburger[1]

[1]Laboratory of Synaptic Mechanisms, Brain Mind Institute, School of Life Science, École Polytechnique Fédérale de Lausanne, 1015 Lausanne, Switzerland, and [2]Blue Brain Project, Brain Mind Institute, School of Life Science, École Polytechnique Fédérale de Lausanne, 1015 Lausanne, Switzerland

Ca^{2+}-dependent transmitter release occurs in a fast and in a slow phase, but the differential roles of Ca^{2+} buffers and Ca^{2+} sensors in shaping release kinetics are still controversial. Replacing extracellular Ca^{2+} by Sr^{2+} causes decreased fast release but enhanced slow release at many synapses. Here, we established presynaptic Sr^{2+} uncaging and made quantitative Sr^{2+}- and Ca^{2+}-imaging experiments at the mouse calyx of Held synapse, to reveal the interplay between Ca^{2+} sensors and Ca^{2+} buffers in the control of fast and slow release. We show that Sr^{2+} activates the fast, Synaptotagmin-2 (Syt2) sensor for vesicle fusion with sixfold lower affinity but unchanged high cooperativity. Surprisingly, Sr^{2+} also activates the slow sensor that remains in Syt2 knock-out synapses with a lower efficiency, and Sr^{2+} was less efficient than Ca^{2+} in the limit of low concentrations in wild-type synapses. Quantitative imaging experiments show that the buffering capacity of the nerve terminal is markedly lower for Sr^{2+} than for Ca^{2+} (~5-fold). This, together with an enhanced Sr^{2+} permeation through presynaptic Ca^{2+} channels (~2-fold), admits a drastically higher spatially averaged Sr^{2+} transient compared with Ca^{2+}. Together, despite the lower affinity of Sr^{2+} at the fast and slow sensors, the massively higher amplitudes of spatially averaged Sr^{2+} transients explain the enhanced late release. This also allows us to conclude that Ca^{2+} buffering normally controls late release and prevents the activation of the fast release sensor by residual Ca^{2+}.

Key words: **calcium buffering capacity; calcium sensor; endogenous fixed buffer; slow release sensor; strontium; synaptotagmin**

Introduction

Ca^{2+}-dependent transmitter release is a fundamental signaling process for fast information transfer between neurons. Release can be separated into a fast phase with a brief duration (<1 ms), followed by a slower phase of up to hundreds of milliseconds. There is good evidence that the fast phase of release is mediated by a rapidly acting Ca^{2+} sensor with a high Ca^{2+} cooperativity, requiring the binding of ~4–5 Ca^{2+} ions before vesicle fusion occurs (Dodge and Rahamimoff, 1967; Goda and Stevens, 1994; Bollmann et al., 2000; Schneggenburger and Neher, 2000). Synaptotagmin-1 (Syt1) functions as the Ca^{2+} sensor for fast release at mouse forebrain synapses and in *Drosophila* (Geppert et al., 1994; Fernández-Chacón et al., 2001; Yoshihara and Littleton, 2002; Pang et al., 2006). Synaptotagmin-2 (Syt2) plays a homologous role as a Ca^{2+} sensor mediating the steeply Ca^{2+}-dependent component of release at a large hindbrain synapses, the calyx of Held (Pang et al., 2006; Sun et al., 2007; Kochubey and Schneggenburger, 2011).

For the slow phase of release, the underlying mechanisms are less clear. Slow release is driven by the spatially averaged $[Ca^{2+}]_i$, which, because of its slower decay (~50 ms), can summate during repeated AP activity. Relating slow release to the measured $[Ca^{2+}]_i$ values in the nerve terminal has shown low apparent Ca^{2+} cooperativities (Delaney and Tank, 1994; Xu-Friedman and Regehr, 2000; Angleson and Betz, 2001), but nonlinear dependencies have been found in other synapses (Ravin et al., 1997; Kirischuk and Grantyn, 2003). Experiments at the calyx synapse have shown that release ~<2 μM is caused by a more linearly acting Ca^{2+} sensor (Lou et al., 2005) that remains in Syt2 KO mice (Sun et al., 2007; Kochubey and Schneggenburger, 2011).

A characteristic feature of fast and slow release is their differential modulation when Ca^{2+} is exchanged by Sr^{2+}, which causes decreased fast release, but increased slow release (Miledi, 1966; Goda and Stevens, 1994; Rumpel and Behrends, 1999; Xu-Friedman and Regehr, 2000). One study has postulated that Sr^{2+} preferentially activates a slow release sensor (Goda and Stevens, 1994). Another study, using imaging of axonal Ca^{2+} and Sr^{2+} transients, showed that Sr^{2+} transients were higher than Ca^{2+} transients and that Sr^{2+} decayed more slowly (Xu-Friedman and Regehr, 1999). They concluded that the differences in release were caused by the slower removal of Sr^{2+} from the nerve terminal (Xu-Friedman and Regehr, 2000). Nevertheless, the absolute values of spatially averaged $[Sr^{2+}]_i$ transients have remained unknown; similarly, quantitative values of the buffering capacity of cells for Sr^{2+} ions are missing. Because there is good agreement that late release is strongly influenced by Ca^{2+} buffering (see

Received May 16, 2014; revised July 11, 2014; accepted July 30, 2014.

Author contributions: N.B., O.K., and R.S. designed research; N.B., O.K., and D.K. performed research; D.K. contributed unpublished reagents/analytic tools; N.B., O.K., and R.S. analyzed data; N.B., O.K., and R.S. wrote the paper.

This work was supported by Swiss National Science Foundation 31003A_138320/1 to R.S. We thank Heather Murray for expert technical assistance, and Erwin Neher for discussing a previous version of the manuscript.

The authors declare no competing financial interests.

Correspondence should be addressed to Dr. Ralf Schneggenburger, Laboratory of Synaptic Mechanisms, Brain Mind Institute, School of Life Science, École Polytechnique Fédérale de Lausanne, 1015 Lausanne, Switzerland. E-mail: ralf.schneggenburger@epfl.ch.

DOI:10.1523/JNEUROSCI.1990-14.2014

 0270-6474/14/3412622-14$15.00/0

Table 1. Sr^{2+} binding affinities of buffers, indicators, and photolyzable chelators used in this study

Buffer	K_d, Ca^{2+}	K_d, Sr^{2+}	Source	Factor Sr^{2+}/Ca^{2+}
CDTA	0.011 μM	4.4 μM	Martell and Smith, 1974	400
EGTA	0.15 μM	35 μM	Martell and Smith, 1974	233
HEDTA	2.5 μM	62 μM	Martell and Smith, 1974	25
ATP	214 μM	724 μM	Wilson and Chin, 1991	3.4
fura-2	0.22 ± 0.007 μM ($n = 3$)	4.8 ± 0.22 μM ($n = 7$)	Calibration	22
fura-4F	1.1 μM	32 ± 0.7 μM ($n = 3$)	Calibration	28
fura-6F	8.4 μM	134 μM	Calibration	16
fura-2FF	6.1 μM	—	Calibration	
DMN	0.005 μM	0.160 μM	Calibration	44

above for references), we argue that quantitative measurements of alien divalent ion buffering, and sensor activation with presynaptic Sr^{2+} and Ca^{2+} uncaging, should yield significant new insights into how Ca^{2+} buffering and Ca^{2+} sensor activation normally shape fast and slow release.

Materials and Methods

Slice preparation and electrophysiology. Acute brainstem slices at the level of MNTB were prepared as described previously (von Gersdorff et al., 1997), using C57BL/6J mice at postnatal days (P) 10–15, or Syt2 $^{-/-}$ mice (Pang et al., 2006) bred on a C57BL6 background, at P12-P15. Mice of either sex were used throughout. Procedures of mouse breeding, handling, and killing before slice preparation were approved by the Veterinary office of the Canton of Vaud, Switzerland. Single or paired whole-cell recordings were made from MNTB principal neurons and/or calyces of Held nerve terminals at room temperature (22°C–24°C), using an EPC-10/2 patch-clamp amplifier (HEKA Elektronik). Series resistances (5–30 MΩ and 3–8 MΩ) were compensated up to 50% and 83% in presynaptic and postsynaptic recordings, respectively. The extracellular solution contained the following (in mM): 125 NaCl, 25 $NaHCO_3$, 2.5 KCl, 1.25 NaH_2PO_4, 25 glucose, 1 $MgCl_2$, 0.4 ascorbic acid, 3 myo-inositol, and 2 Na-pyruvate (all from Sigma-Aldrich/Fluka), continuously bubbled with 95% O_2/5% CO_2 (pH 7.4; 310 mosm), to which either 2 mM $CaCl_2$ or 2 mM $SrCl_2$ was added. During the afferent fiber stimulation experiments (see Fig. 2), 10 μM bicuculline methochloride (Biotrend) and 2 μM strychnine (Sigma) were added to suppress inhibitory synaptic currents. Afferent fibers were stimulated using a custom-built platinum/iridium bipolar electrode placed at the midline of the brainstem slice, with 2–10 V pulses of 0.1 ms length from an isolated stimulator (A-M Systems, model 2100). During paired recordings, the following chemicals were added to the extracellular solution: 10 mM tetraethylammonium chloride (TEA, Sigma), 1 μM TTX, 50 μM D-AP5, 2 mM γ-D-glutamylglycine, and 100 μM cyclothiazide (all from Biotrend). The postsynaptic pipette solution contained the following (in mM): 130 Cs-gluconate, 20 TEA, 10 HEPES, 5 Na_2-phosphocreatine, 4 MgATP, 0.3 Na_2GTP, 5 EGTA (pH 7.2 adjusted with CsOH). The presynaptic pipette solution for double recordings without imaging (see Fig. 3) was identical, except for a reduced concentration of EGTA (100 μM). The presynaptic intracellular solution for divalent ion uncaging and imaging experiments, referred to as "imaging solution" below, contained the following (in mM): 130 Cs-gluconate, 20 TEA, 20 HEPES, 5 Na_2ATP, 0.3 Na_2GTP (pH 7.2 adjusted with CsOH). To this, 1.5 or 1 mM DM-Nitrophen (DMN, Merck Chemicals), $CaCl_2$ or $SrCl_2$ to achieve 90% loading, and/or 100 μM of a fura2-like indicator were added.

Quantitative presynaptic divalent imaging and uncaging. We established presynaptic quantitative Sr^{2+} uncaging by using DMN (Ellis-Davies, 2003) and ratiometric fura-2 and fura-4F indicators (Invitrogen) for postflash $[Sr^{2+}]_i$ imaging (see Figs. 4 and 5). Titration experiments with 100 μM fura-2 to measure free Sr^{2+} (data not shown) gave a K_d value for Sr^{2+} binding to DMN of 160 nM (Table 1; ~40 times higher than for Ca^{2+}). Fura-2 and fura-4F were calibrated for Sr^{2+} binding in the presence of DMN (1.5 mM) using a 5-point calibration procedure (Fig. 1). For this, suitable free Sr^{2+} concentrations were set by mixtures of $SrCl_2$ with CDTA, EGTA, or HEDTA using published Sr^{2+} affinities for these buffers (Martell and Smith, 1974) (Table 1), in the presence of 100 μM fura-4F and 1.5 mM DMN. Fluorescence spectra were then measured in the experimental setup using the same optical path and excitation parameters as in Sr^{2+} uncaging experiments, using 50 μm path length borosilicate glass capillaries (VitroCom). Figure 1 shows an example for Sr^{2+} calibration of fura4F, revealing a K_d of 31.9 μM. In all calibrations, at least one Sr^{2+} concentration was determined by two independent buffers (in the example of Fig. 1, EGTA and HEDTA for a free $[Sr^{2+}]$ close to 20 μM). All calibrations for Ca^{2+} and Sr^{2+} were performed using the imaging solution supplemented with 100 μM of the fura2-like dye, 1.5 mM DMN, and $CaCl_2$ or $SrCl_2$ DMN as appropriate. The amount of $CaCl_2$ or $SrCl_2$ to be added was calculated based on our estimates of the DMN stock purity (usually ~65%).

For presynaptic Ca^{2+} and Sr^{2+} uncaging experiments, a xenon arc flash lamp (SP-20, Rapp OptoElectronic) with 395 nm short-pass filter was used to generate short (0.4–0.5 ms half-width) UV light flashes to induce DMN photolysis. The flashlight was fiber-coupled into the microscope together with the light from a monochromator (Polychrome IV, TILL Photonics) using an 85%/15% beamsplitter (TILL Photonics), and the flash intensity was modulated by neutral density filters (Rapp OptoElectronic). For imaging postflash $[Ca^{2+}]_i$ and $[Sr^{2+}]_i$ following weak flashes, we used fura-2, whereas fura-2FF (TEFLabs) or fura-4F was used for stronger flashes for Ca^{2+} and Sr^{2+}, respectively (see Fig. 4C; Table 1). Ratiometric measurements of preflash and postflash $[Ca^{2+}]_i$ and $[Sr^{2+}]_i$ were made using alternating 5 ms excitation light pulses from the monochromator at 380 and 350 nm. In Sr^{2+} uncaging experiments, the extracellular solution contained 2 mM $SrCl_2$ (no added $CaCl_2$), to avoid the possibility of Ca^{2+} leak into the presynaptic cell. When DMN was used without added Sr^{2+} or Ca^{2+} in the presence of 2 mM extracellular Sr^{2+}, neither ratiometric changes nor release responses were observed upon full intensity flashes ($n = 3$ cells). This suggests that these responses were caused by Sr^{2+} release from DMN and not by a possible Ca^{2+} contamination.

Presynaptic buffered loading of divalent ions. To measure the divalent ion sensitivity of release close to the resting concentrations of Ca^{2+} or Sr^{2+} (see Fig. 6), we loaded calyx nerve terminals with buffered Ca^{2+} or Sr^{2+} solutions in paired presynaptic and postsynaptic recordings (Lou et al., 2005). For Sr^{2+}, we used 0.3, 1.6, and 5 mM $SrCl_2$ mixed with 10 mM CDTA and 100 μM fura-2 in the imaging solution, giving nominal free $[Sr^{2+}]$ values of 0.14, 0.83, and 4.3 μM, respectively. For Ca^{2+}, we used buffered solutions with 10 mM EGTA and nominal $[Ca^{2+}]$ of 0.12, 0.31, and 0.85 μM. The effective presynaptic $[Ca^{2+}]_i$ and $[Sr^{2+}]_i$ was imaged continuously during the recording using fura-2 ratio measurements every 5 s, and the mEPSC frequency was simultaneously sampled by the postsynaptic recording.

Measurements of presynaptic Ca^{2+} and Sr^{2+} buffering capacity. For measuring the endogenous Sr^{2+} buffering capacity, $\kappa_S(Sr)$ (see Fig. 7), we attempted to compete with endogenous buffers by adding buffering capacity of the indicator dye (κ_B) during the loading phase of whole-cell recordings (Neher and Augustine, 1992). To do so, we used 75 and 200 μM of the high-affinity indicator fura-2 for the determination of κ_S for Ca^{2+} and Sr^{2+}, respectively. At these concentrations and considering the binding affinities of fura-2 for Ca^{2+} and Sr^{2+} (Table 1), fura-2 will attain final κ_B values of ~350 for Ca^{2+} and ~50 for Sr^{2+}. Measurements of κ_S were then performed as described previously (Neher and Augustine, 1992; Helmchen et al., 1997), using repeated presynaptic depolar-

izations of 3 ms to 0 mV (see Fig. 7*A*,*B*). Fura-2 ratios in response to depolarizations were measured at 380 nm wavelength and at the isosbestic wavelengths, which were 357 and 362 nm for Ca^{2+} and Sr^{2+}, respectively, using alternating 5 ms monochromator light pulses. For the determination of κ_S (Sr), 2 mM extracellular Sr^{2+} was present throughout the experiment. The offline analysis started by extracting the ratio F_{380}/F_{357} (or F_{380}/F_{362}) following suitable background correction. Ratio traces were then converted to $[Ca^{2+}]_i$ or $[Sr^{2+}]_i$ according to the equation of Grynkiewicz et al. (1985), using experimentally determined calibration constants R_{min}, R_{max}, and K_{eff}. Endogenous buffering capacity (κ_S) and extrusion rates (γ) for Ca^{2+} and Sr^{2+} were estimated similarly as described before for Ca^{2+} (Neher and Augustine, 1992; Helmchen et al., 1997).

Imaging of physiological Ca^{2+} and Sr^{2+} transients. For the experiments in Figure 8, we used the lowest-affinity Ca^{2+} indicator practical for ratiometric measurements, fura-6F (Invitrogen). Given the K_d values of fura-6F for Ca^{2+} and Sr^{2+} (Table 1), 100 μM fura-6F corresponds to κ_B values of ~12 for Ca^{2+} and < 1 for Sr^{2+}. Because these values are severalfold smaller than the cellular buffering capacities κ_S for each ion (see Fig. 7), fura-6F does not significantly influence the kinetics of Sr^{2+} and Ca^{2+} transients. Ratiometric measurements were made before, during, and after trains of 50 AP-like presynaptic depolarizations (1 ms to 45 mV at 100 Hz), using alternating 10 ms pulses of monochromator light at 380 and 350 nm at repetition rates of initially 8 Hz and then 41 Hz to follow fast changes of $[Ca^{2+}]_i$ or $[Sr^{2+}]_i$ (see Fig. 8). Fluorescence ratio traces were converted into $[Ca^{2+}]_i$ or $[Sr^{2+}]_i$ time courses as explained above. The extracellular recording solution contained 1 μM TTX and 10 mM TEA.

Data analysis. Data analysis was done using custom-written routines in IgorPro 6.2 (WaveMetrics). Spontaneous mEPSC events were detected using a semiautomatic routine with a template-matching algorithm (Clements and Bekkers, 1997). EPSC deconvolution followed the methods introduced by Neher and Sakaba (2001), as described previously (Wölfel et al., 2007). The quantal size for deconvolution was set by the average mEPSC amplitude determined in each cell. Release rates were corrected for the predicted "spillover" current estimated using "template" protocols, which consisted of a few presynaptic depolarizations of different length applied at the beginning of paired recordings (Neher and Sakaba, 2001). In case of Syt2 $^{-/-}$ recordings, template protocols were not helpful because of the absence of synchronous release; thus, the strength of residual current β was set to values between 10 and 20, similar to those observed in control synapses from the same age group. The cumulative release rate traces after uncaging were fitted with single-exponential, exponential plus line, double-exponential, double-exponential plus line, and triple-exponential functions with a fit routine (Wölfel et al., 2007; Kochubey et al., 2009). In wild-type synapses with uncaging steps > 4 μM $[Ca^{2+}]_i$ or ~>15 μM $[Sr^{2+}]_i$, the best fits usually contained two exponential components (see Fig. 4*A*,*B*, bottom; and Fig. 4*E*, open and closed symbols). In Syt2 $^{-/-}$, the best fit was usually monoexponential and much slower (~200 ms; see Fig. 5*A*, bottom).

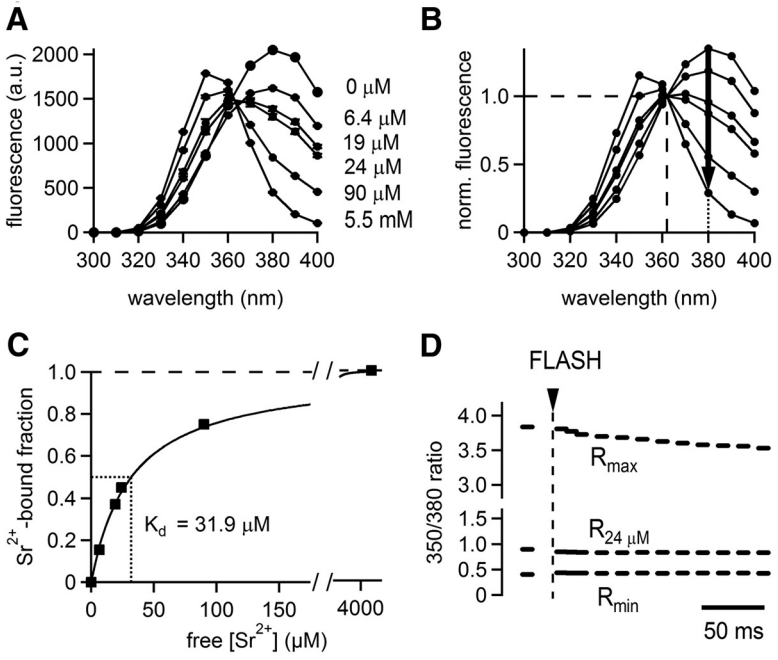

E

added Sr^{2+} (mM)	buffer	free $[Sr^{2+}]$ (μM)
0	EGTA (10mM)	0
3.6	EGTA (10mM)	6.4
5.8	EGTA (10mM)	19.2
29.8	HEDTA (100mM)	24
10	EGTA (10mM)	90
10	not added	5483

F

	before flash	after flash
R_{min}	0.42	0.43
$R_{24\mu M}$	0.9	0.85
R_{max}	3.84	3.81
K_{eff}	153.17	184.68

Figure 1. Example of a Sr^{2+} calibration measurement of fura-4F. ***A***, Excitation spectra of fura-4F experimentally obtained in a set of buffered Sr^{2+} calibration solutions. Each curve is the average of three repetitions. ***B***, The same set of spectra after normalization to the isosbestic point (dashed lines; 362 nm). For each $[Sr^{2+}]$, the fluorescence decrement at 380 nm was divided by its maximal value (indicated by the arrow) to calculate the Sr^{2+}-bound fura-4F fraction. ***C***, Sr^{2+}-bound fraction of fura-4F as a function of free Sr^{2+} concentration (symbols). The fit with a Michaelis–Menten function (line) yielded $K_d = 31.9$ μM. Note that fura-4F binding affinity to Sr^{2+} is much lower than that for Ca^{2+} (~1.1. μM; Table 1). ***D***, The solutions with the lowest and highest $[Sr^{2+}]$ and a 24 μM $[Sr^{2+}]_{free}$ solution buffered with high HEDTA were used to determine the calibration parameters R_{min}, R_{max}, and K_{eff} for the ratiometric determination of pre- and postflash $[Sr^{2+}]_i$. Shown are the fura-4F fluorescence ratios measured *in vitro* at 350 and 380 nm excitation, using the same illumination protocol as in the presynaptic Sr^{2+} uncaging experiments. Each data point is an average of three repetitions. ***E***, Table summarizing the content of Sr^{2+} calibration solutions. For calculating free $[Sr^{2+}]$, 1.5 mM DMN, 100 μM fura-4F, and 5 mM ATP contained in the solutions were considered in addition to the specified buffer, using the dissociation constants listed in Table 1. ***F***, Preflash and postflash values of the fura-4F calibration ratios R_{min}, R_{max}, and $R_{24\mu M}$, and of the third calibration parameter K_{eff} calculated from the three calibration ratios, assuming DMN photolysis efficiency of 80%.

Data are reported as mean ± SEM, unless indicated. Paired or unpaired Student's *t* tests, as appropriate, were used to assess statistical significance.

Model calculations. We modeled the Ca^{2+} and Sr^{2+} sensitivity of transmitter release obtained from uncaging experiments with the "2-sensor model" (see Fig. 4*F*) (Sun et al., 2007), or with an allosteric model of Ca^{2+} binding and vesicle fusion (Lou et al., 2005). For fitting the Ca^{2+} and Sr^{2+} uncaging data in Syt2 $^{-/-}$ synapses (see Fig. 5), we assumed that release can be described by a slow sensor with a single divalent ion binding site (see Fig. 5*F*). The set of differential equations corresponding to each model was solved numerically with the fourth- or fifth-order Runge-Kutta method in IgorPro, calculating the accumulation into the various fused states for a series of Ca^{2+} and Sr^{2+} steps. Ca^{2+} and Sr^{2+} steps decayed by 30% per 100 ms similar to observed steps (see Fig. 4*A*,*B*). We derived the release rate traces by differentiation of the simulated cumulative release traces and then analyzed the peak release rate, release delay (time to release of 5 vesicles), and release time constants.

Table 2. Parameters of the 2-sensor model fitted to the Sr^{2+} and Ca^{2+} uncaging data in wild-type synapse

	Ca^{2+}	Sr^{2+}	Factor Sr^{2+}/Ca^{2+}
Fast sensor			
k_{on} ($M^{-1}s^{-1}$)	2.6×10^8	1.2×10^8	0.46
k_{off} (s^{-1})	6808	19,000	2.79
K_d (k_{off}/k_{on})	26 μM	158 μM	6.07
γ_F (s^{-1})	6900	6900	1
b (cooperativity factor)	0.5	0.5	1
No. of sites	5	5	1
Slow sensor			
k_+ ($M^{-1}s^{-1}$)	1.5×10^5	0.5×10^5	0.33
k_- (s^{-1})	323	520	1.61
K_d (k_{off}/k_{on})	2.1 mM	10.4 mM	4.95
γ_S (s^{-1})	28.5	28.5	1
No. of sites	1	1	1
Spontaneous release			
γ_0 (s^{-1})	5.8×10^{-4}	5.8×10^{-4}	1

The Ca^{2+} and Sr^{2+} sensitivities of peak release rate, release delay, and fast component of the release time constants were then globally fitted by the 2-sensor model (see Figs. 4*C–E*; Fig. 6*B*). We lowered the Ca^{2+} and Sr^{2+} binding affinities of the slow release sensor relative to the values found in Syt2 KO measurements (see Fig. 5), to account for "clamping" of the slow sensor by Syt2 in wild-type synapses (Table 2). The back-calculation of local $[Ca^{2+}]_i$ and $[Sr^{2+}]_i$ signals evoked by a single AP (see Fig. 9) was done as described previously (Kochubey et al., 2009).

The stochastic model of divalent ion influx and buffering (see Fig. 9*E*) was performed by the Monte Carlo simulator M-Cell (Kerr et al., 2008). The total simulated volume was a cube measuring $0.6 \times 0.6 \times 1.2$ μm. The Sr^{2+} current through single Ca^{2+} channels was scaled to a factor of 1.8 that of Ca^{2+} flux (see Fig. 3); the Ca^{2+} current was 0.12 pA at 0 mV. Ca^{2+} channels were modeled using a Hodgkin–Huxley model (Borst and Sakmann, 1998) driven by an action potential with a half-width of 0.49 ms. We assumed the presence of the following buffers, with on-rates (k_{on}) and off-rates (k_{off}) for Ca^{2+} and Sr^{2+}, respectively: (1) an endogenous immobile ("fixed") Ca^{2+} buffer; k_{on} 1×10^8 and 4×10^7 $M^{-1}s^{-1}$ and k_{off} 1000 and 2500 s^{-1}. The K_d values of the endogenous immobile buffer for Ca^{2+} and Sr^{2+} were 10 and 62.5 μM, respectively, achieved by using a 0.4-fold lower k_{on} and a 2.5-fold higher k_{off} for Sr^{2+} compared with Ca^{2+}. Given the concentration of the buffer (400 μM), this corresponds to cellular buffer capacities κ_S of 40 and 6.4 for Ca^{2+} and Sr^{2+}, respectively, close to the experimentally observed values (see Fig. 7). (2) ATP was present as a mobile Ca^{2+} buffer (Naraghi and Neher, 1997) at a concentration of 2 μM; k_{on} $5 \times 10^8/5 \times 10^8$ $M^{-1}s^{-1}$ (for Ca^{2+}/Sr^{2+}, respectively), k_{off} 45,000/152,242 s^{-1}. The lower affinity for Sr^{2+} was as found in previous experiments (Wilson and Chin, 1991) (Table 1). ATP also bound Mg^{2+} with k_{on} of 5×10^8 $M^{-1}s^{-1}$ and k_{off} of 22,500 s^{-1}; free $[Mg^{2+}]$ was 300 μM. The diffusion constant of free Sr^{2+} was 2.2×10^{-6} cm^2/s, and the basal free $[Sr^{2+}]$ was 100 nM.

Results

Sr^{2+} decreases AP evoked release probability but increases late asynchronous release

Previous studies have shown that phasic release during the presynaptic AP is reduced in the presence of Sr^{2+}, whereas a late phase of release is increased (Miledi, 1966; Goda and Stevens, 1994; Rumpel and Behrends, 1999; Xu-Friedman and Regehr, 1999). Here, we used the ideal presynaptic accessibility of the calyx of Held synapse to perform direct measurements of the Sr^{2+} sensitivity of release and of Sr^{2+} buffering, to gain new insights into how Ca^{2+} buffering and Ca^{2+} sensor activation normally shape fast and slow release. We started by investigating the effects of Ca^{2+} replacement by Sr^{2+} on fiber-stimulation-evoked EPSCs. We used brief 100 Hz trains of 50 stimuli to study both AP-evoked fast release during the train and late asynchronous release after the train (Fig. 2*A1*, *A2*). When the extracellular Ca^{2+} was switched to Sr^{2+} (2 mM each), the first EPSC during 100 Hz trains was strongly reduced, from 20.4 ± 0.4 nA to 5.2 ± 0.5 nA (Fig. 2*A*,*B*; $n = 5$ cells; $p < 0.01$). The relative speed of depression was reduced (Fig. 2*B*), which is likely a consequence of a lower release probability p_{rel} in the presence of Sr^{2+}. To quantify p_{rel}, we estimated the size of the readily releasable pool using high-frequency stimulation trains and cumulative EPSC amplitude plots (Fig. 2*B*) (Schneggenburger et al., 1999). The pool size was slightly, but significantly, decreased in the presence of Sr^{2+} (~20%; Fig. 2*C*; $p < 0.05$). Dividing the first EPSC amplitude by the readily releasable pool showed that p_{rel} was strongly reduced in the presence of Sr^{2+} (Fig. 2*C*; $p < 0.001$). The cumulative EPSC amplitude plots also showed a reduced late slope, which corresponds to a reduced EPSC amplitude between the 30th and 50th stimuli (Fig. 2*B*, *C*). This could indicate a reduced Ca^{2+}-dependent readily releasable pool recovery in the presence of Sr^{2+} (Wang and Kaczmarek, 1998; Sakaba and Neher, 2001), which was not further analyzed here. Together, replacing Ca^{2+} with Sr^{2+} decreased the EPSC amplitude, an effect that was caused by a reduced p_{rel}.

We next analyzed the late asynchronous release following the 100 Hz trains (Fig. 2*A2*). Late release, measured as mEPSC frequency, was significantly enhanced during the first 1 s interval after the train (2 mM Ca^{2+}, 20.5 ± 6.8 Hz; 2 mM Sr^{2+}; 143.5 ± 11.8 Hz; $p < 0.01$). During the second and third 1 s time intervals, release was still enhanced, although the difference was smaller (Fig. 2*A2* bottom; $p < 0.05$ for both comparisons). This reveals a differential effect of Ca^{2+} replacement by Sr^{2+}, with less phasic but enhanced late asynchronous release, as shown previously at other synapses.

Sr^{2+} decreases fast release rates despite carrying larger currents through Ca^{2+} channels

We next wished to investigate the mechanism that underlies the lower efficiency of extracellular Sr^{2+} in activating fast transmitter release. Using paired presynaptic and postsynaptic whole-cell recordings, we found that Sr^{2+} currents through presynaptic voltage-gated Ca^{2+} channels were increased (Fig. 3*A*), suggesting that Sr^{2+} is a better charge carrier than Ca^{2+} (Hagiwara and Ohmori, 1982). Despite the higher Sr^{2+} currents, pool-depleting 50 ms depolarizations caused smaller EPSCs, and deconvolution of EPSCs showed that peak release rates were smaller in the presence of Sr^{2+} (Fig. 3*A*, bottom, *B*). Fitting the cumulative release rates with double-exponential functions, we also found that the number of vesicles released in the fast phase was reduced, and the fast release time constant was slowed from an average value of 1.3 ms to ~2.3 ms (Fig. 3*C*; $p < 0.01$ for both comparisons). These data show that, despite an increased flux of Sr^{2+} through Ca^{2+} channels, the fast release component in response to presynaptic depolarizations was activated less efficiently by Sr^{2+} than by Ca^{2+}.

Sr^{2+} activates the fast release sensor with sixfold lower efficiency than Ca^{2+}

We next wished to investigate the mechanisms that underlie a lower efficiency of extracellular Sr^{2+} in activating fast release. Because Sr^{2+} permeates more readily through Ca^{2+} channels (factor of ~1.8-fold; see Fig. 3*B*), the microdomain intracellular Sr^{2+} concentration attained close to open Ca^{2+} channels should be higher in the presence of Sr^{2+} than Ca^{2+}, as we will also show below (see Fig. 9). Therefore, Sr^{2+} might activate the Ca^{2+} sensor

for fast release significantly less efficiently than Ca^{2+}, a likely possibility that, however, has never been tested directly.

To study the intracellular Sr^{2+} sensitivity of transmitter release, we next established Sr^{2+} uncaging experiments at the calyx of Held synapse. This required an accurate calibration of all involved fura2-like Ca^{2+} indicators and of DMN for Sr^{2+} (see Materials and Methods; Fig. 1). For all chelators and indicators calibrated here, we found lower affinities for Sr^{2+} than for Ca^{2+} (Table 1) (Xu-Friedman and Regehr, 1999). The low affinity of fura-4F for Sr^{2+} (~31 μM) turned out to be very useful for imaging $[Sr^{2+}]_i$ in the range of 20–100 μM, following Sr^{2+} uncaging pulses. Figure 4*A* shows an example of a paired recording with 1.5 mM DMN (90% loaded with Sr^{2+}) and 0.1 mM fura-4F in the presynaptic patch pipette. A full intensity flash led to a $[Sr^{2+}]_i$ elevation of ~50 μM; under similar conditions with 1.5 mM Ca^{2+}-loaded DMN, smaller rises in free $[Ca^{2+}]_i$ are observed (~10–20 μM $[Ca^{2+}]_i$; Fig. 4*A*,*B*). We attribute this difference to the significantly lower Sr^{2+} buffering capacity of the nerve terminal (see also below, Fig. 7). These experiments show the feasibility to control presynaptic $[Sr^{2+}]_i$ in Sr^{2+} uncaging experiments at a CNS nerve terminal.

Presynaptic Sr^{2+} uncaging experiments showed that, despite higher presynaptic $[Sr^{2+}]_i$ steps, EPSCs and peak release rates were smaller compared with Ca^{2+} uncaging experiments (Fig. 4*A*,*B*), suggesting a lower efficiency of intracellular Sr^{2+} at the Ca^{2+} sensor for vesicle fusion. Plotting the peak release rates as a function of postflash $[Ca^{2+}]_i$ and $[Sr^{2+}]_i$ indeed revealed a clear, ~6-fold rightward shift in the efficiency of Sr^{2+} in inducing transmitter release (Fig. 4*C*). Interestingly, the slopes in the steep parts of the double-logarithmic dose–response curves, determined by line fitting of the data points in double-logarithmic space, were similar for Ca^{2+} and Sr^{2+} uncaging (3.42 ± 0.37 and 3.50 ± 0.24 over the ranges 1–5 μM and 5–25 μM, respectively; error estimates are 95% confidence interval of the fits). Fits of the data with a modified 2-sensor model of release (Sun et al., 2007) (Fig. 4*F*) or with an allosteric release model (Lou et al., 2005) were consistent with an ~6-fold rightward shift of the affinity of Sr^{2+} binding to the fast sensor (Fig. 4*C*, solid and dashed lines, respectively). The Sr^{2+} data were described well by 5 divalent ion binding sites and an unchanged cooperativity factor b (Table 2), in agreement with the finding of unchanged slopes in double-logarithmic coordinates.

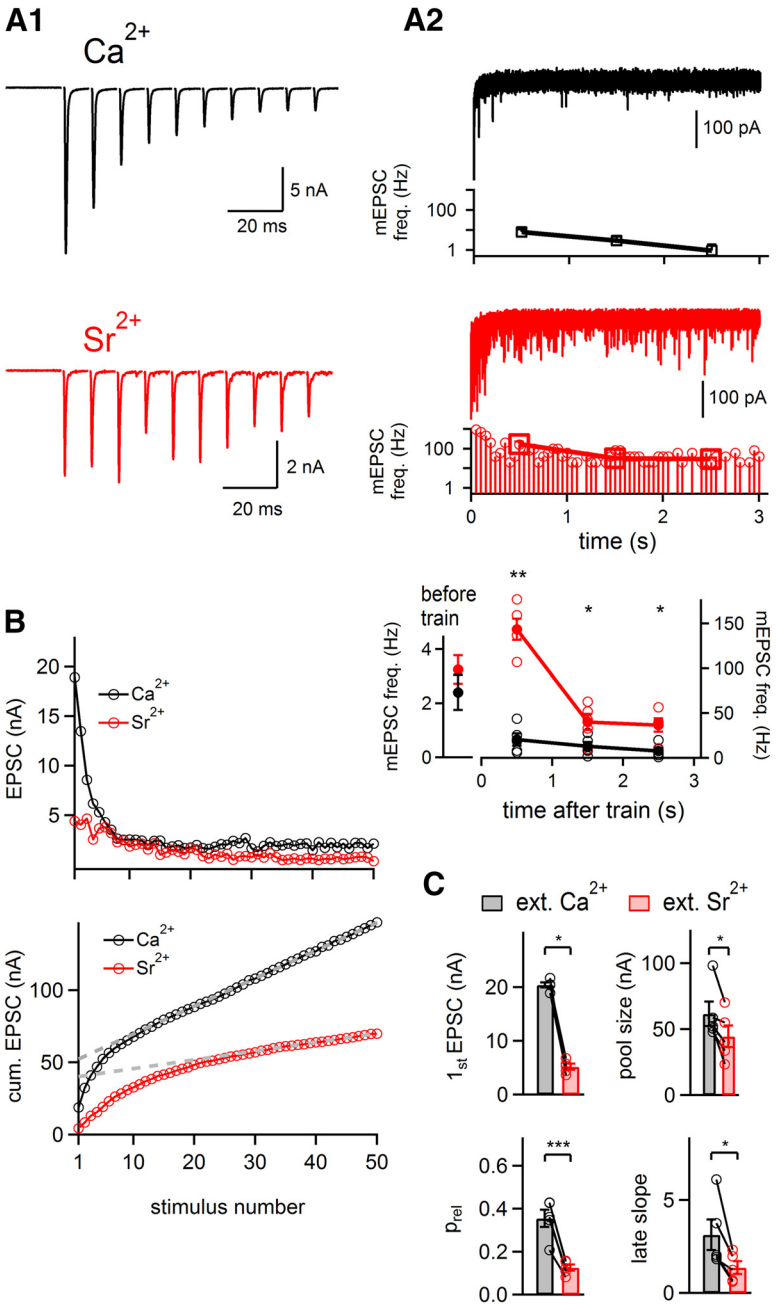

Figure 2. Reduced fast release but increased asynchronous release upon substitution of extracellular Ca^{2+} with Sr^{2+}. ***A***, Examples of afferent fiber stimulation-evoked train of EPSCs (***A1***; 50 APs, 100 Hz) recorded initially in the presence of 2 mM external Ca^{2+} (black trace), and after replacing Ca^{2+} with Sr^{2+} (red trace). Stimulation artifacts were blanked. Current traces on the right (***A2***) show the late release activity during a 3 s interval, and corresponding mEPSC frequency plots. mEPSC frequency analyses before and after 100 Hz trains (***A2***, bottom), show that Sr^{2+} markedly increased the asynchronous release rate after the train ($n = 4$ cells). The baseline mEPSC frequency before the train was not significantly changed in the presence of Sr^{2+} ($p = 0.34$). In this and all subsequent figures, black and red traces and data symbols represents data obtained in the presence of Ca^{2+} and Sr^{2+}, respectively. *$p < 0.05$. **$p < 0.01$. ***B***, Plots of peak EPSC amplitudes (top) and cumulative EPSCs (bottom) as a function of stimulus number during 100 Hz trains, both in the presence of 2 mM Ca^{2+} and after switching the extracellular solution to 2 mM Sr^{2+}. Back-extrapolation of line fits to the late part of the cumulative EPSC plot indicates approximately similar pool size, despite a different late slope. Dividing the first EPSC amplitude by the pool size provides an estimate for initial release probability (p_{rel}). ***C***, Individual and average values for the first EPSC amplitude; pool size; p_{rel}; and the late slope, each in the presence of 2 mM Ca^{2+} or Sr^{2+}. Note that the decreased first EPSC amplitude (by ~75%) is, to a large part, explained by the decreased p_{rel} (~60% relative decrease; $p < 0.001$). *$p < 0.05$. ***$p < 0.001$.

We next analyzed the kinetic components of release induced by Sr^{2+} and Ca^{2+} uncaging to determine the kinetics of Sr^{2+} binding to the fast release sensor. The release delays with Sr^{2+} uncaging steps showed a clear rightward shift (Fig. 4*D*). Cumu-

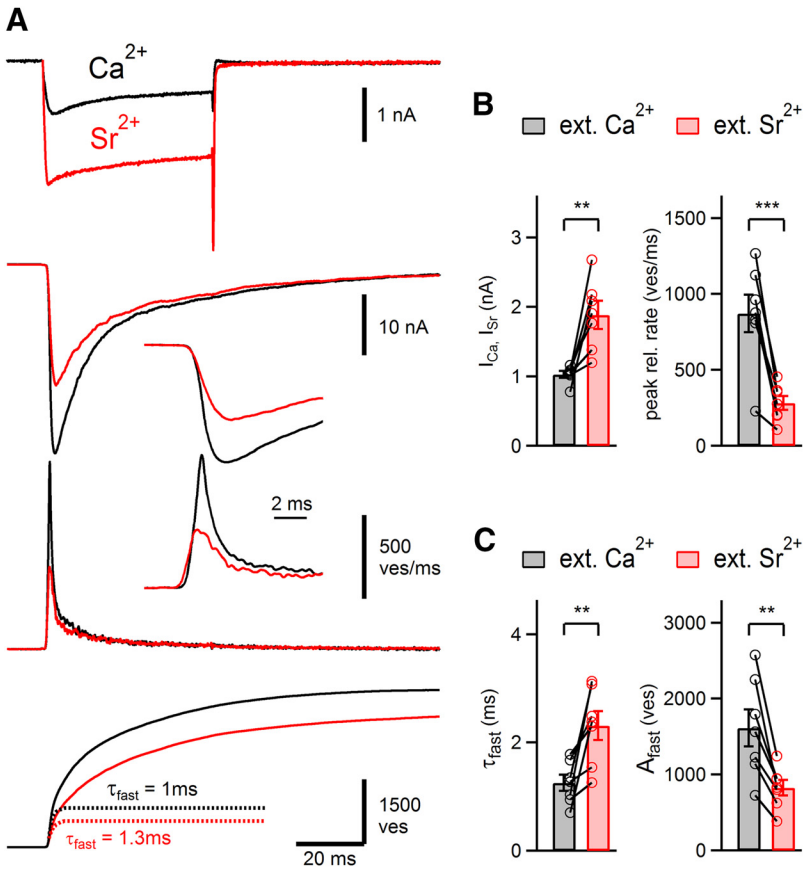

Figure 3. Fast release is reduced in the presence of Sr^{2+} despite a twofold larger presynaptic depolarization-evoked influx of Sr^{2+}. ***A***, Presynaptic Ca^{2+} and Sr^{2+} currents, and the transmitter release kinetics in response to these stimuli, were studied in paired presynaptic and postsynaptic recordings. Top to bottom, Presynaptic Ca^{2+} and Sr^{2+} currents in the presence of extracellular Ca^{2+} and Sr^{2+} (2 mM each); postsynaptic EPSCs and transmitter release rates; and cumulative release traces with the isolated mono-exponential fit components (dashed lines). Despite the increased currents carried by Sr^{2+} through the presynaptic voltage-gated Ca^{2+} channels (top), the transmitter release rates were reduced in the presence of Sr^{2+}. ***B***, Individual and average values of peak presynaptic Ca^{2+} and Sr^{2+} currents with steps to 0 mV (left; $p < 0.01$), and of peak transmitter release rates (right; $p < 0.001$; $n = 7$ paired recordings each). $^{**}p < 0.01$. $^{***}p < 0.001$. ***C***, Individual and average values of estimated fast release time constant (left, $p < 0.01$) and of the number of vesicles released in the fast component (right, $p < 0.01$; $n = 7$ paired recordings each). Note the smaller peak release rates (***B***) and slower release time constant τ_{fast} in the presence of Sr^{2+} compared with Ca^{2+}. $^{**}p < 0.01$.

lative release rates in response to both Ca^{2+} and Sr^{2+} uncaging followed double-exponential functions (Fig. 4*A*,*B*, bottom) (Wölfel et al., 2007). The fast and the slow release time constants were significantly rightward shifted with Sr^{2+} compared with Ca^{2+} (Fig. 4*E*). Global fits of the 2-sensor model to the peak release rates, the release delays, and the fast release time constants (Fig. 4*C–E*) showed a decreased on-binding rate (k_{on}), as well as an increased dissociation rate k_{off} for Sr^{2+} relative to Ca^{2+}, whereas the vesicle fusion rate γ_F of the fast sensor was left unchanged (Table 2). The parameters of the slow sensor (S in Fig. 4*F*) were fixed according to the data obtained at low $[Sr^{2+}]_i$ and $[Ca^{2+}]_i$, which will be presented below (see Fig. 6). Taken together, presynaptic divalent ion uncaging shows that Sr^{2+} has a sixfold rightward shifted affinity at the fast release sensor compared with Ca^{2+}. This is explained by a lower k_{on} and by a higher k_{off} for Sr^{2+} (Table 2). However, the intrinsic cooperativity of Ca^{2+} and Sr^{2+} ions in evoking fast release is unchanged.

Sr^{2+} is less efficient at the slow release sensor remaining in Syt2 KO mice

We have shown above that the fast Ca^{2+} sensor at the calyx of Held has a significantly lower affinity for Sr^{2+} compared with Ca^{2+}. Because replacement of Ca^{2+} by Sr^{2+} causes decreased phasic release but enhanced asynchronous release (Fig. 2), it has been suggested that Sr^{2+} preferentially activates the slow release sensor (Goda and Stevens, 1994). To investigate this possibility directly, we made Sr^{2+} uncaging experiments in Syt2 KO mice. The low-cooperativity release component that remains in Syt2 KO mice is driven by a secondary release sensor, which might represent the slow release sensor in wild-type synapses (Sun et al., 2007; Kochubey and Schneggenburger, 2011) (see Discussion).

In Syt2 KO mice at P12-P15, Ca^{2+} uncaging stimuli evoked slowly rising EPSCs with small peak release rates of ~1–20 ves/ms depending on postflash $[Ca^{2+}]_i$ (Fig. 5*A*). Cumulative release rates in Syt2 KO mice showed a sigmoidal rise, and their relaxation after ~50 ms could be fitted with single exponential functions with time constants ~200 ms (Fig. 5*A*), much slower than in wild-type synapses (see above; Fig. 4). With Sr^{2+} uncaging, we found even lower peak release rates and slower release (Fig. 5*B*). When we plotted peak release rates, release time constants, and release delays as a function of divalent ion concentrations, we found a clear right shift with Sr^{2+} as compared to with Ca^{2+} (Fig. 5*C–E*). These measurements directly show that Sr^{2+} activates the slow sensor studied in Syt2 KO mice with lower efficiency compared with Ca^{2+}.

To describe the Ca^{2+} and Sr^{2+} uncaging data in Syt2 KO mice quantitatively, we developed a kinetic model for the slow release sensor. For this, we first fitted the Ca^{2+} and Sr^{2+} dependencies of peak release rates in double-logarithmic coordinates by line functions, which revealed slopes of 0.85 ± 0.11 and 0.90 ± 0.14 (95% confidence intervals; see Fig. 5*C*, dashed lines). Because the cooperativity was <1, we developed a kinetic model with a single divalent ion binding site (Fig. 5*F*). A global fit of this model to the Sr^{2+} and Ca^{2+} dependencies of peak release rates, release time constants, and release delays indicated that Sr^{2+} elicited slow release with a 5.5-fold rightward shifted affinity compared with Ca^{2+} (Fig. 5*C*). The model fits indicated that the rightward shift was caused by a lower binding rate constant k_{on} (~4.8-fold; for parameters, see legend of Fig. 5). These experiments demonstrate that, even at the slow sensor, Sr^{2+} is less efficient than Ca^{2+}, and the factor is similar to the one we found for Syt2 in wild-type mice (Fig. 4).

At low concentrations, Sr^{2+} also triggers release less efficiently than Ca^{2+}

We have shown that Sr^{2+} has a significantly lower efficiency at the slow release sensor which remains in Syt2 KO synapses. However, in the absence of Syt2, slow release is increased, indicating that Syt2 normally "clamps" slow release (Yoshihara and Littleton, 2002; Kochubey and Schneggenburger, 2011). It is possible

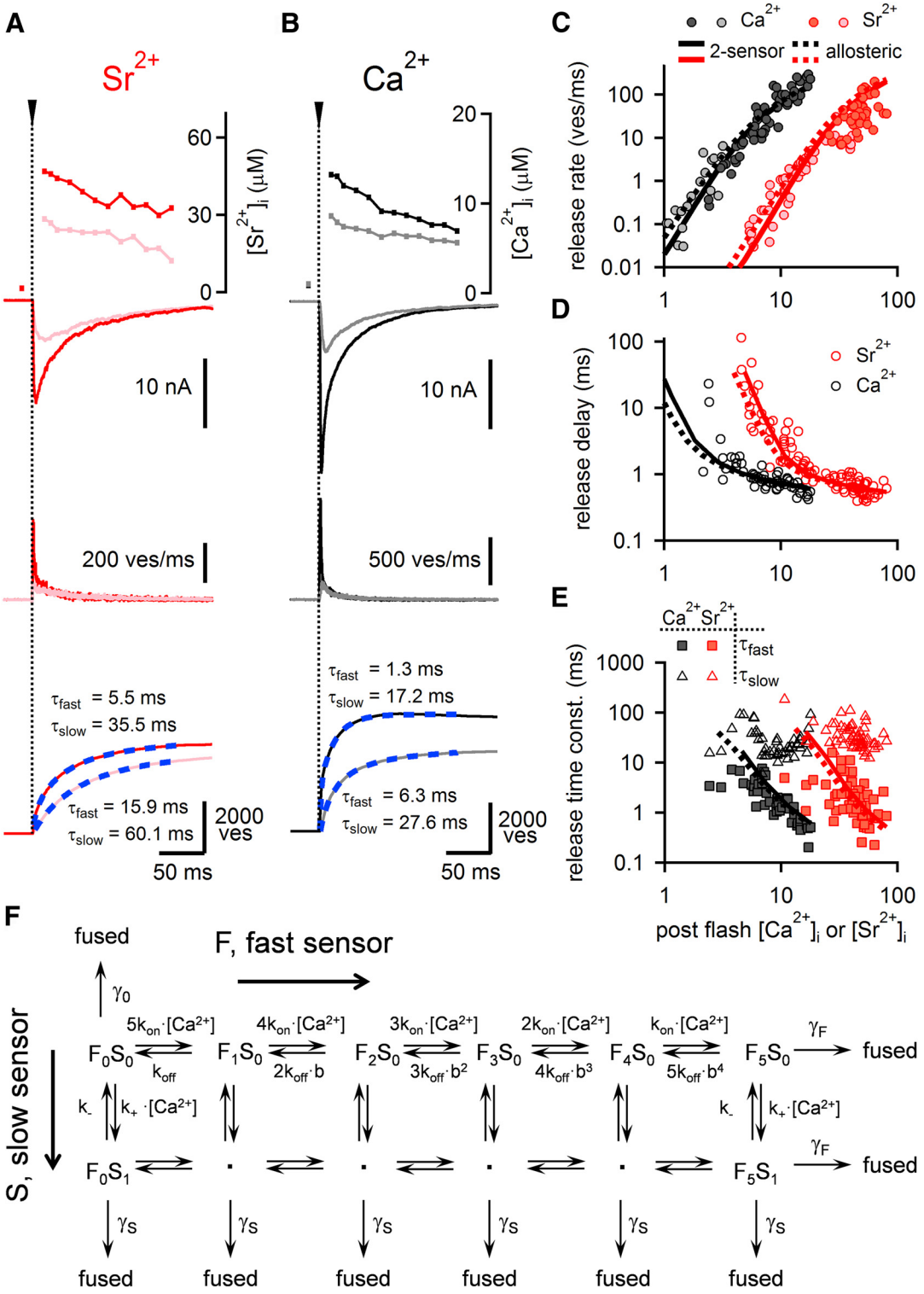

Figure 4. The intrinsic Sr^{2+} sensitivity of release is lower than for Ca^{2+} but divalent ion cooperativity is unchanged. ***A***, ***B***, Example Sr^{2+} and Ca^{2+} uncaging experiments. Top to bottom panels, Presynaptic $[Sr^{2+}]_i$ and $[Ca^{2+}]_i$ traces during two subsequent flashes; the postsynaptic EPSC; transmitter release rates derived from the EPSCs; and cumulative release rates with overlaid best fit functions (dashed lines; double-exponential, or double exponential plus line functions; τ_{fast} and τ_{slow} values are indicated). ***C***, ***D***, Plots of peak release rates (***C***) and of release delays (***D***) for both Sr^{2+} and Ca^{2+} uncaging experiments (black and red symbols, respectively). Data were obtained in the presence of fura-2 (light symbols), and fura-2FF or fura-4F (dark symbols) for Ca^{2+} or Sr^{2+}, respectively. The fits of the data with the 2-sensor model (solid lines) or with the allosteric model (dashed lines) are superimposed. Note the strong, ~6-fold rightward shift of peak release rates (***C***) and the longer release delays in the Sr^{2+} uncaging data (***D***). ***E***, Plot of the Sr^{2+} and Ca^{2+} sensitivity of the fast and slow release time constants, for those cumulative release traces that were best fitted by double-exponential functions (~>10 μM, or 4 μM $[Sr^{2+}]_i$ and $[Ca^{2+}]_i$, respectively). Filled and open symbols represent fast and slow time constants, respectively. The fit predictions of the 2-sensor model and of the allosteric model, with the same set of parameters as used for the fits in (***C***, ***D***), are superimposed (sold and dashed lines, respectively). For the fit parameters found for the 2-sensor model, see Table 2. Note the rightward shift of the fast release time constant τ_{fast}, and τ_{slow} with Sr^{2+} as compared to Ca^{2+}. ***F***, Scheme of the 2-sensor model for divalent ion binding and vesicle fusion used to fit the data. The kinetic rates for divalent binding assumed in the allosteric model (for the kinetic scheme, see Lou et al., 2005) were $k_{on} = 2.3 \times 10^8$ and $1.1 \times 10^8\ M^{-1}s^{-1}$, $k_{off} = 6800$ and $19{,}000\ s^{-1}$ for Ca^{2+} and Sr^{2+}, respectively; the other parameters were the same: $b = 0.45$, $l_+ = 5.85 \times 10^{-4}\ s^{-1}$, $f = 25.96$, pool size 1710 vesicles.

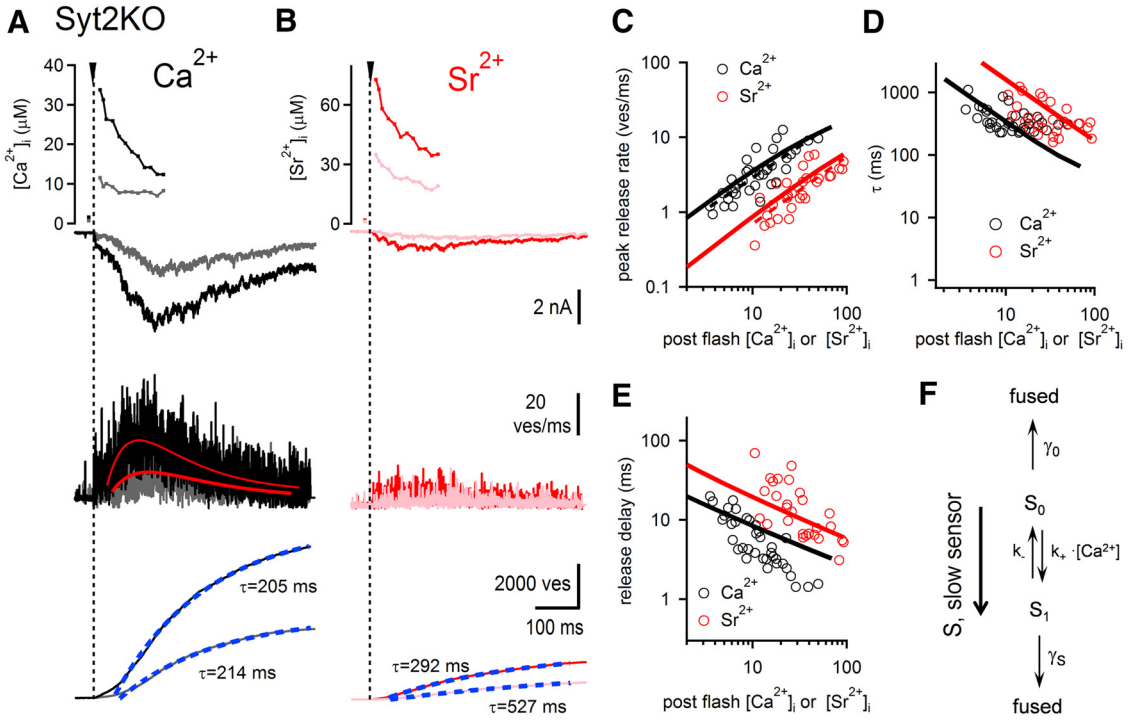

Figure 5. Sr^{2+} is also less efficient at the slow sensor that remains at the calyx of Held synapses from Syt2 KO mice. ***A***, ***B***, Examples for Ca^{2+} and Sr^{2+} uncaging experiments with (top to bottom) postflash $[Ca^{2+}]_i$ and $[Sr^{2+}]_i$ transients, EPSCs, release rates, and cumulative release traces. The latter were fitted with single exponential functions with time constants (τ) as indicated. ***C–E***, Dependence of peak release rates (***C***), release time constants (***D***), and release delays (***E***) on postflash $[Ca^{2+}]_i$ and $[Sr^{2+}]_i$ (black and red symbols, respectively). All three datasets for each divalent ion were globally fitted with the slow sensor model shown in ***F***. ***F***, Scheme of the slow sensor release model with a single divalent ion binding site used to fit the data in ***C–E***. The parameters used for the fits in ***C–E*** were as follows: $k_+ = 3.85 \times 10^5$ and $0.8 \times 10^5\ \mu M^{-1} s^{-1}$ for Ca^{2+} and Sr^{2+}, respectively; $k_- = 7.56\ s^{-1}$, $\gamma_S = 28.5\ s^{-1}$, $\gamma_0 = 5.85 \times 10^{-4}\ s^{-1}$.

that the unclamped slow sensor in the absence of Syt2 has altered Ca^{2+}- or Sr^{2+}-binding properties. Therefore, we next measured the intracellular Sr^{2+} sensitivity of release in the low concentration range in wild-type mice. Because train stimulation elevates residual divalent ion concentrations to the low micromolar range (see below; Fig. 8), understanding how Ca^{2+} and Sr^{2+} regulate vesicle fusion in this concentration range is immediately relevant to explain late asynchronous release following trains of APs.

We loaded presynaptic calyx of Held nerve terminals with Sr^{2+}-buffered solutions using CDTA (10 mM) as a Sr^{2+} buffer and various concentrations of $SrCl_2$, to achieve elevated levels of presynaptic $[Sr^{2+}]_i$ (see Materials and Methods). We then imaged the spatially averaged $[Sr^{2+}]_i$ attained in calyces using 100 μM Fura-2 while simultaneously measuring the rate of spontaneous release (Fig. 6*A*) (Lou et al., 2005). These measurements showed that below ~5 μM $[Sr^{2+}]_i$, the slope in the double-logarithmic plot of release rate versus $[Sr^{2+}]_i$ progressively decreased (Fig. 6*B*, pink square symbols), similarly as shown previously for Ca^{2+} (Lou et al., 2005; Sun et al., 2007). The Sr^{2+} data fell below, and on the right of corresponding measurements with Ca^{2+} (Fig. 6*B*, gray square symbols). At low concentrations of each divalent ion in the range of 30–100 nM, release rates converged to the resting spontaneous release frequency, which is ~1 Hz at the calyx of Held. These data suggest that Sr^{2+} activates the slow release sensor in wild-type synapses with lower efficiency compared with Ca^{2+}.

The data obtained in the range of low intracellular Ca^{2+} and Sr^{2+} concentrations allowed us to fit the 2-sensor model to the Ca^{2+} and Sr^{2+} datasets (Fig. 6*B*). We assumed that the slow sensor has a single divalent ion binding site, based on the slope value of ~1 revealed in the Syt2 KO experiments (see above; Fig. 5). Furthermore, for the fit of the wild-type data in Figure 6, we had to introduce "clamping" of the slow sensor because Syt2 suppresses the activation of the slow sensor (Kochubey and Schneggenburger, 2011). This was done by introducing an additional factor to decrease the affinity of the slow sensor for both Ca^{2+} and Sr^{2+} in wild-type synapses (Fig. 6; for the model parameters, see Table 2). The data and the fits clearly show that, in the range of high divalent ion cooperativity, which is dominated by Syt2, Sr^{2+} is ~6-fold less efficient in triggering vesicle fusion than Ca^{2+}. At lower divalent ion concentrations, this difference becomes smaller; but at all concentrations down to ~100 nM, Sr^{2+} is less efficient than Ca^{2+} in driving release.

Using the 2-sensor model with the fitted parameters, we could predict the contributions of release occurring without previous divalent ion binding (spontaneous release), and release occurring after occupancy of the slow and the fast release sensor (Fig. 6*C*). Surprisingly, this indicates that late release measured after 100 Hz trains in the presence of Sr^{2+} (Fig. 2; 150 Hz) might be carried by a larger relative activation of the fast sensor. This is because release in the presence of extracellular Sr^{2+} extends more strongly into the steep part of the dose–response curve compared with Ca^{2+} (Fig. 6*B*, broken lines) (see Discussion).

The intracellular buffering capacity for Sr^{2+} is severalfold lower than for Ca^{2+}

Because Sr^{2+} is less efficient at both the fast and the slow release sensors, the explanation for the significantly larger late release in the presence of Sr^{2+} must lie in a higher rise of spatially averaged Sr^{2+} compared with Ca^{2+}. This might be caused by inefficient intracellular buffering of Sr^{2+} ions and/or by a slower decay of spatially averaged Sr^{2+}, as concluded previously (Xu-Friedman and Regehr, 1999). However, quantitative information on how high spatially averaged Sr^{2+} rises in the nerve terminal, and on

the Sr^{2+} buffering capacity of cellular cytosol has not been obtained. For this reason, we next measured the Sr^{2+} buffering capacity of the calyx nerve terminal, using the indicator overload method (Neher and Augustine, 1992; Helmchen et al., 1997). This again required careful calibration of fura-2 for Sr^{2+} (see Materials and Methods).

We loaded calyces with 200 μM fura-2 in the presence of 2 mM extracellular Sr^{2+} and stimulated the nerve terminals repeatedly with brief depolarizations (0 mV for 3 ms; Fig. 7*A*, inset). The first stimulus during whole-cell recordings, when only little fura-2 had entered the nerve terminal, induced large $[Sr^{2+}]_i$ transients (Fig. 7*A*, arrow). During the loading phase of calyces with fura-2, the $[Sr^{2+}]_i$ transients progressively decreased in amplitude, indicating increasing competition of fura-2 with the cellular buffering mechanism (Fig. 7*A*), similarly as previously demonstrated for Ca^{2+} (Neher and Augustine, 1992). Using the K_d value of Sr^{2+} binding to fura-2 as determined in calibration measurements ($K_d \sim 4.2$ μM; Table 1), and the Sr^{2+}-independent fura-2 fluorescence as a proxy of the intracellular fura-2 concentration, we calculated the exogenously added Sr^{2+} buffering capacity of fura-2, κ_B (Sr), for each stimulus. Plots of the inverse of the $[Sr^{2+}]_i$ amplitude against κ_B (Sr) indicated an endogenous buffering capacity for Sr^{2+}, κ_S (Sr), of 6 in this recording. The extrapolated $[Sr^{2+}]_i$ transient at zero added exogenous buffer was ~8 μM (Fig. 7*C*, arrows).

In parallel experiments, we measured the buffer capacity for Ca^{2+}, κ_S (Ca), using 75 μM fura-2 in the patch pipette and 2 mM extracellular $[Ca^{2+}]$. Despite similar divalent ion charge (Fig. 7*A*,*B*, insets), the free $[Ca^{2+}]_i$ transients were significantly smaller, ~≤0.5 μM. As a consequence, the inverse amplitudes of the free divalent concentration transients were significantly larger for Ca^{2+} than for Sr^{2+} (Fig. 7*B*,*D*). This indicates a higher buffering capacity for the nerve terminal for Ca^{2+} compared with Sr^{2+}. On average, κ_S (Ca) was 46 ± 2.8 ($n = 5$ cells), whereas κ_S (Sr) was only 8.5 ± 0.6 ($n = 11$ cells; $p < 0.001$; Fig. 7*F*). This massive difference is most likely caused by a lower binding affinity of endogenous fixed buffers for Sr^{2+} compared with Ca^{2+} (see Discussion). The back-extrapolated amplitude of the $[Sr^{2+}]_i$ transient was 12 ± 0.84 μM ($n = 10$), >10-fold higher than the back-extrapolated $[Ca^{2+}]_i$ amplitude, which was 0.89 ± 0.05 μM (Fig. 7*F*, middle; $n = 5$, $p < 0.001$). This difference was not caused by larger currents carried by Sr^{2+} through Ca^{2+} channels because, in these particular experiments, the divalent ion charge was similar (Fig. 7*F*, right). These experiments are, to our knowledge, the first measurement of intracellular Sr^{2+} buffering capacity in any cell type. They show that the Ca^{2+} buffering system of the nerve terminal has an ~5- to 6-fold lower capacity for Sr^{2+} compared with Ca^{2+}. This admits a massively higher spatially averaged $[Sr^{2+}]_i$ (Figs. 7*A*, arrow, and see Fig. 8).

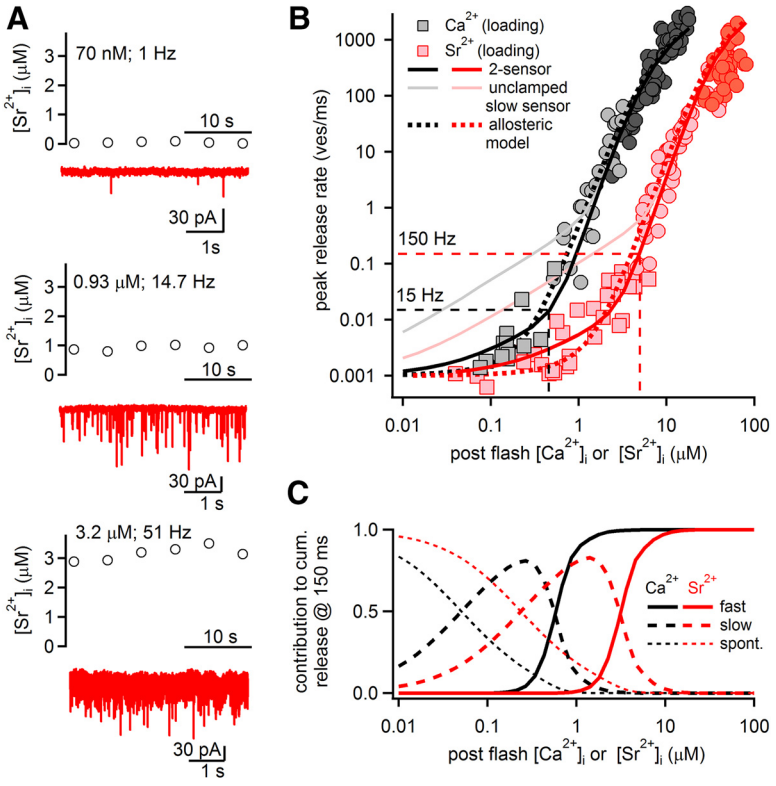

Figure 6. Sr^{2+} is less efficient than Ca^{2+} at low intracellular concentrations in wild-type synapses. ***A***, Calyces of wild-type mice were loaded with CDTA-buffered Sr^{2+} solutions with different free $[Sr^{2+}]$. The resulting effective $[Sr^{2+}]_i$ was measured by fura-2 ratio imaging (open symbols), whereas the release activity was continuously measured in postsynaptic recordings of mEPSCs (bottom). ***B***, The Sr^{2+} and Ca^{2+} sensitivities of transmitter release over a wide range of divalent ion concentration. The pink and gray square data points indicate the release rates measured at low intracellular Sr^{2+} and Ca^{2+} concentrations (***A***). The round data points are from the divalent ion uncaging experiments (replotted from Fig. 4*C*; same meaning of symbols). Note the double-logarithmic scales and the shallower slope at low divalent ion concentrations. The fits of the Ca^{2+} and Sr^{2+} sensitivity of release by the 2-sensor model (solid lines) and by the allosteric model (dotted lines) are superimposed. The pink and the gray solid lines indicate the prediction of the 2-sensor model using the affinity for Ca^{2+} and Sr^{2+} as measured in Syt2 KO calyces (Fig. 5). For the final 2-sensor model, the affinities for Ca^{2+} and Sr^{2+} at the slow sensor were reduced ~100-fold to explain "clamping" of the slow sensor in the presence of Syt2 (Kochubey and Schneggenburger, 2011) (Table 2). The horizontal dashed lines indicate the measured release rates after high-frequency stimulation (Fig. 2); vertical dashed lines indicate the predicted $[Ca^{2+}]_i$ and $[Sr^{2+}]_i$ values. ***C***, Prediction of the 2-sensor model of the origin of fused vesicles. Release was tracked as originating from the unoccupied sensor ("spontaneous"; rate γ_0 in the scheme of the 2-sensor model in Fig. 4*F*); from the occupied slow sensor ("slow"; rate γ_S); or else, release upon full occupancy of the fast sensor ("fast"; γ_F).

We next analyzed the Sr^{2+} extrusion rate constant compared with Ca^{2+} using the fura-2 overload data in Figure 7. For this purpose, we plotted the decay time constants of the $[Sr^{2+}]_i$ and $[Ca^{2+}]_i$ transients as a function of the corresponding κ_B values for Ca^{2+} and Sr^{2+} (Fig. 7*E*). Interestingly, the extrapolated values of the $[Ca^{2+}]_i$ and $[Sr^{2+}]_i$ decay time constants for zero exogenous buffer were quite similar (~90–100 ms; Fig. 7*E*, arrow; *y*-axis intercept). However, the slope of the plot of τ versus κ_B was much higher for Sr^{2+} than for Ca^{2+}, which indicates a significantly lower extrusion rate γ for Sr^{2+} (Fig. 7*E*,*G*; ~4.2-fold; $p < 0.001$). Thus, the similar extrapolated value of τ_{decay} for $[Sr^{2+}]_i$ and $[Ca^{2+}]_i$ for no added exogenous buffers is caused by a compensation of the smaller extrusion rate constant γ by the significantly smaller endogenous buffering capacity for Sr^{2+}, κ_S (Sr), resulting in similar time constants of decay. Taken together, fura-2 overload experiments establish that the endogenous divalent ion buffering capacity of the nerve terminals is drastically lower for Sr^{2+} than for Ca^{2+}.

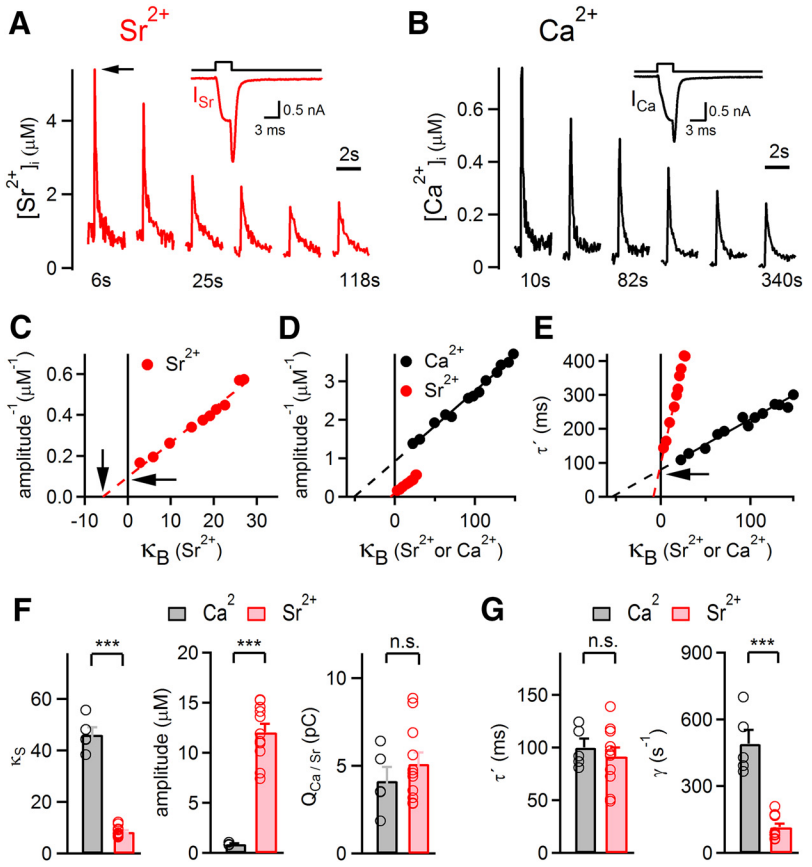

Figure 7. The intracellular buffering capacity for Sr^{2+} in the nerve terminal is much weaker than for Ca^{2+}. ***A***, ***B***, Example of fura-2 loading experiments in which the presynaptic terminal was repeatedly depolarized to 0 mV for 3 ms (insets) to induce Sr^{2+} (***A***) or Ca^{2+} (***B***) influx, whereas an increasing concentration of fura-2 filled the recorded nerve terminal during the first ~300 s of whole-cell recording of a calyx of Held. Subsequent traces of $[Sr^{2+}]_i$ and $[Ca^{2+}]_i$ transients in response to the depolarizations at different times of whole-cell recordings are shown. ***C***, ***D***, Plots of inverse peak amplitude versus exogenously added buffer capacity (κ_B) for $[Sr^{2+}]_i$ (***C***), or for $[Sr^{2+}]_i$ and $[Ca^{2+}]_i$ (***D***). ***E***, Plots of the $[Sr^{2+}]_i$ and $[Ca^{2+}]_i$ decay time constants as a function of κ_B for Sr^{2+} and Ca^{2+}. ***C–E***, Data are from the same recordings as shown in ***A***, ***B***. ***F***, Average and individual values for endogenous buffer capacity κ_S (left), for the peak divalent ion transient extrapolated to the beginning of whole-cell recording (middle), and for the divalent ion charge entering during the 3 ms depolarization (right). Data for Sr^{2+} and Ca^{2+} are shown. Note an ~5.5-fold smaller buffering capacity for Sr^{2+} compared with Ca^{2+} (left; $p < 0.001$), and the much larger $[Sr^{2+}]_i$ transient amplitude (middle; $p < 0.001$). ***G***, Average and individual values of the extrapolated decay time constant, τ' of divalent ion transients (left), and of the divalent ion extrusion rate γ (right), for both Sr^{2+} and Ca^{2+}. Note the significantly smaller γ for Sr^{2+} compared with Ca^{2+} ($p < 0.001$). ***$p < 0.001$. n.s., Not significant.

Spatially averaged $[Sr^{2+}]_i$ elevations are much higher than $[Ca^{2+}]_i$

The significantly lower buffering capacity of the presynaptic cytosol for Sr^{2+} is expected to cause a drastically larger buildup of free Sr^{2+} compared with Ca^{2+}. To investigate the Ca^{2+} and Sr^{2+} signals relevant for the late phase of release observed after high-frequency trains (Fig. 2), we performed quantitative Ca^{2+} and Sr^{2+} imaging experiments following 100 Hz trains of AP-like stimulations. We used a low-affinity indicator (fura-6F; 100 μM) to image physiologically relevant divalent ion transients while only minimally perturbing their amplitude or kinetics (see Materials and Methods).

In presynaptic voltage-clamp recordings, we first imaged $[Ca^{2+}]_i$ in response to 100 Hz trains of AP-like voltage-clamp depolarizations (Fig. 8*A*) and then switched the extracellular solution to Sr^{2+} (2 mM in both cases; Fig. 8*A*, *B*). The peak $[Sr^{2+}]_i$ transient reached at the end of the 100 Hz trains was 33.0 ± 3.5 μM, drastically higher than $[Ca^{2+}]_i$, which was 3.6 ± 0.4 μM (Fig. 8*C*, left; $p < 0.001$). Part of this difference was caused by the larger Sr^{2+} currents through Ca^{2+} channels (Fig. 8*A*,*B*, inset). The larger part of the ~10-fold higher $[Sr^{2+}]_i$ transients compared with $[Ca^{2+}]_i$ must be caused by the significantly lower buffering capacity of the nerve terminal for Sr^{2+} compared with Ca^{2+} (~5.5-fold; Fig. 7). We fitted the decay of the $[Sr^{2+}]_i$ and $[Ca^{2+}]_i$ transients with exponential plus line functions (Fig. 8*A*,*B*, dashed lines). This showed a significant difference of the decay time τ (Fig. 8*C*, middle; $p < 0.01$), but the values were close, consistent with the results of Figure 7*E*. The late residual $[Sr^{2+}]_i$ signal, measured at a time of 3τ, was, however, >10-fold higher than the corresponding $[Ca^{2+}]_i$ value (Fig. 8*C*, right; 4.6 ± 0.5 and 0.28 ± 0.03 μM, respectively; $n = 5$; $p > 0.001$). The large difference between the absolute values of $[Sr^{2+}]_i$ and $[Ca^{2+}]_i$ becomes clearer by direct overlay of two representative traces recorded in the same cell (Fig. 8*B*). Thus, the spatially averaged $[Sr^{2+}]_i$ rises to ~10-fold higher values than $[Ca^{2+}]_i$ both during and after the train. This difference is, to a large part, caused by a significantly smaller buffering capacity κ_S of the nerve terminal for Sr^{2+}.

The microdomain Sr^{2+} signal is not strongly affected by the weaker Sr^{2+} buffering

We finally wished to investigate whether the lower buffering capacity of the nerve terminal for Sr^{2+} would also affect the "local" Sr^{2+} signal relevant for phasic release. For this purpose, we first back-calculated the local Ca^{2+} and Sr^{2+} concentrations relevant for AP-driven fast release, based on the measured intracellular Ca^{2+} and Sr^{2+} sensitivities of release (Fig. 4) (for the back-calculation approach, see Schneggenburger and Neher, 2000). We recorded single EPSCs in response to afferent fiber stimulation in the presence of Ca^{2+} and then exchanged the bath solution to Sr^{2+}. As expected, the EPSC amplitudes and peak release rates were smaller in the presence of Sr^{2+} (Fig. 9*A*,*B*). Nevertheless, the back-calculation approach returned larger local $[Sr^{2+}]_i$ signals compared with Ca^{2+} (Fig. 9*C*), which reflects the lower efficiency of intracellular Sr^{2+} at the fast sensor (Fig. 4). On average, the amplitudes of the local Ca^{2+} and Sr^{2+} transients were 18.4 ± 1.98 μM and 38.9 ± 4.2 μM, respectively ($n = 5$ cells; $p < 0.001$; Fig. 9*D*), which corresponds to a relative increase of 2.12 ± 0.11-fold. This factor approximately reflects the increased Sr^{2+} flux through open Ca^{2+} channels (~1.8-fold; Fig. 3*B*), suggesting that the lower buffering capacity measured for spatially averaged Sr^{2+} transients (Fig. 7) has only little influence on the brief "local" Sr^{2+} signal relevant for phasic release. This might be caused by the fact that endogenous fixed buffers will be rapidly saturated locally by incoming divalent ions (Roberts, 1994; Naraghi and Neher, 1997).

To validate the role of the divalent ion buffer in controlling the local Ca^{2+} and Sr^{2+} signals, we performed random-walk simu-

lations of Ca^{2+} and Sr^{2+} influx and buffering at a release site (Fig. 9*E*), assuming that the κ_S-like buffer is represented by an endogenous fixed buffer with relatively low affinity (see Discussion). We used an array of several Ca^{2+} channels because release at the calyx of Held synapse is controlled by multiple Ca^{2+} channels (Meinrenken et al., 2002; Wang et al., 2009). With the chosen distances, a brief local Ca^{2+} transient with amplitude of ~25 μM was found, in good agreement with the experimental observations (Fig. 9*D*) (Schneggenburger and Neher, 2000). To model the local Sr^{2+} signal, three modifications were made in the simulation, based on our experimental observations. First, the influx through Ca^{2+} channels was increased 1.8-fold. Second, the affinity of the endogenous immobile buffer was reduced 6.25-fold, as derived from our measurements of the reduced buffer capacity. Third, the divalent ion binding parameters for the mobile buffer ATP, which was also present in these simulations, were adapted to previously published Sr^{2+} values (see Materials and Methods). This resulted in a peak local Sr^{2+} signal of ~60 μM; and in repeated simulations, the local Sr^{2+} signal was 2.38 ± 0.04-fold higher than Ca^{2+} (n = 95 repetitions), in good agreement with the back-calculation approach. We conclude that the lower affinity of the endogenous fixed buffer for Sr^{2+} does not have a large effect on the microdomain divalent ion concentration in the presence of Sr^{2+}.

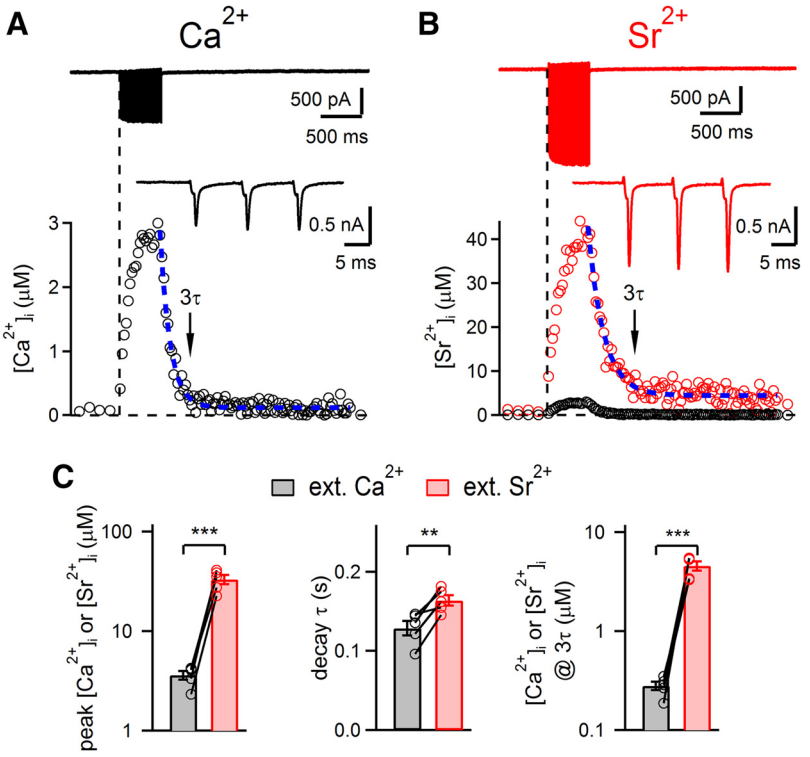

Figure 8. Spatially averaged Sr^{2+} rises to 10-fold higher values than Ca^{2+}. ***A***, ***B***, Presynaptic current (top) and traces of $[Ca^{2+}]_i$ and $[Sr^{2+}]_i$ (bottom; ***A*** and ***B***, respectively) in response to 100 Hz AP-like presynaptic depolarizations. Initially, 2 mM Ca^{2+} was present in the bath solution (***A***), which was subsequently replaced with 2 mM Sr^{2+} (***B***). Insets, Presynaptic Ca^{2+} and Sr^{2+} currents. Blue dashed lines indicate exponential fits to the decay phases of spatially averaged $[Ca^{2+}]_i$ and $[Sr^{2+}]_i$ signals. ***B***, Black trace replots the $[Ca^{2+}]_i$ trace shown in ***A***, to illustrate the massively higher intracellular free $[Sr^{2+}]_i$ rise. ***C***, Individual and average values of peak intracellular divalent ion concentration during the 100 Hz train (left), decay time constant (middle), and divalent ion concentration remaining at a time of 3·τ (right) (n = 5 paired comparisons each). Note the significantly, ~10 times higher peak and late $[Sr^{2+}]_i$ values compared with $[Ca^{2+}]_i$ (left and right; $p < 0.001$ for both comparisons). **$p < 0.01$. ***$p < 0.001$.

Discussion

We have used quantitative presynaptic Ca^{2+} and Sr^{2+} uncaging and imaging at the calyx of Held of wild-type and Syt2-deficient mice, to probe the divalent ion regulation of fast and slow transmitter release. Sr^{2+} uncaging showed that the highly cooperative Ca^{2+} sensor in wild-type synapses has a sixfold lower affinity for Sr^{2+} compared with Ca^{2+} but an unchanged steep slope value (Fig. 4). We show that Sr^{2+} also activates the slow sensor that remains in Syt2 KO synapses less efficiently than Ca^{2+} (Fig. 5) and that Sr^{2+} triggers release less efficiently than Ca^{2+} in the low concentration range (Fig. 6). Thus, the enhanced slow release in the presence of Sr^{2+} must be caused by a significantly higher spatially averaged $[Sr^{2+}]_i$ in the nerve terminal, to overcome the lower efficiency of Sr^{2+} at both release sensors. Indeed, we found that spatially averaged $[Sr^{2+}]_i$ rises to ~10-fold higher values than $[Ca^{2+}]_i$ (Fig. 8), in large part caused by a significantly lower buffering capacity of the nerve terminal for Sr^{2+} compared with Ca^{2+} (Fig. 7). Thus, replacing Ca^{2+} with Sr^{2+} illuminates the roles of Ca^{2+} sensing and Ca^{2+} buffering in controlling fast and slow release, and allows us to conclude that endogenous fixed buffers normally suppress asynchronous release in the nerve terminal.

Using presynaptic Sr^{2+} uncaging experiments, we showed that Sr^{2+} activates fast release with a drastically rightward shifted affinity, but unchanged cooperativity compared with Ca^{2+} (Fig. 4). Although it was somewhat expected that Sr^{2+} has a lower affinity at the fast sensor given the reduced amount of fast release in the presence of Sr^{2+}, this premise has not been shown directly in intracellular ion uncaging experiments at synapses (but see Kishimoto et al., 2001). A previous study used measurements of EPSCs in hippocampal autaptic neurons cultured from Syt1 mutant mice and wild-type mice in the presence of Ca^{2+} and Sr^{2+}, and additional biochemical experiments, and concluded that the Sr^{2+} action in fast release is caused by Sr^{2+} binding to the C2B domain (Shin et al., 2003). This view agrees with mutational analysis at various preparations, including the calyx of Held, which showed that neutralization of aspartate residues in the C2B domain abolished the steeply Ca^{2+}-dependent release component (Mackler et al., 2002; Nishiki and Augustine, 2004; Kochubey and Schneggenburger, 2011). Interestingly, the unchanged cooperativity that we demonstrated here for the action of Sr^{2+} suggests that Sr^{2+} binding could be used to study mechanisms by which Syt1 and Syt2 mediate the steeply Ca^{2+}-dependent component of release, which is a hallmark of fast transmitter release at synapses.

Using Sr^{2+} uncaging in Syt2 KO mice, we showed that the remaining slow release sensor is also activated less efficiently by Sr^{2+} than Ca^{2+} (~5- to 6-fold). This shows that the slow sensor does not preferentially bind Sr^{2+}, opposite to a previous postulate (Goda and Stevens, 1994). Rather, enhanced late release in the presence of extracellular Sr^{2+} must be caused by a significantly reduced Sr^{2+} buffering compared with Ca^{2+}. This conclusion significantly extends beyond the previous axonal imaging

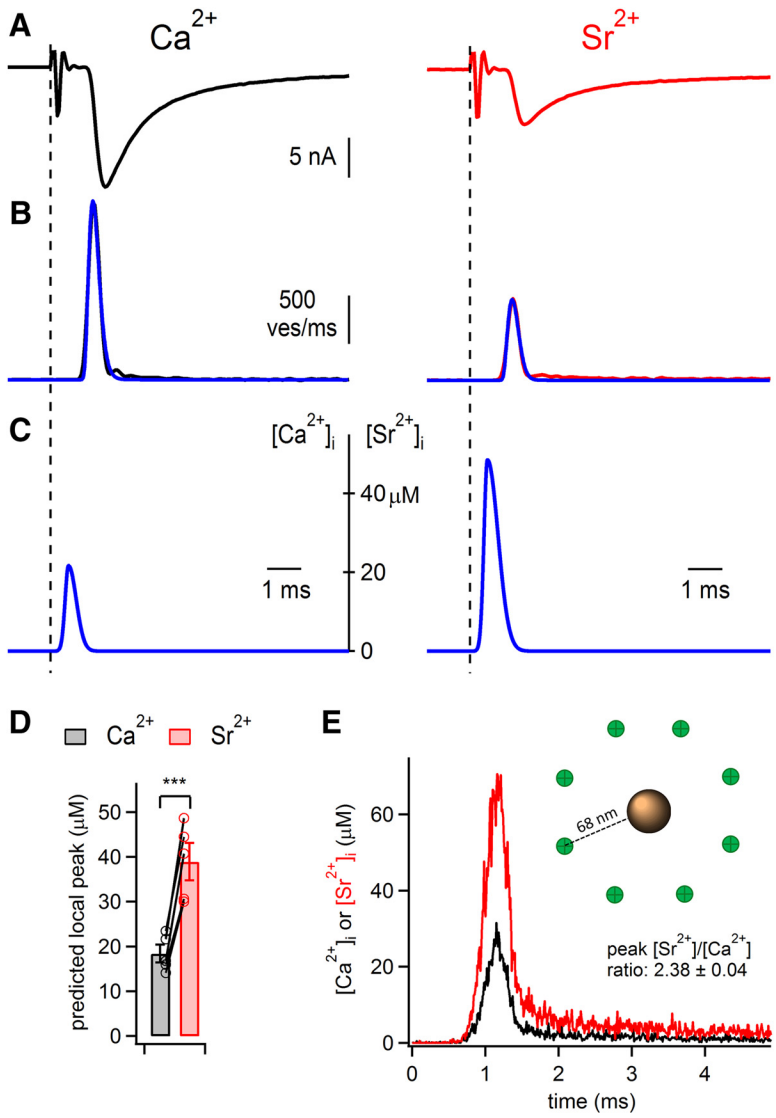

Figure 9. The local $[Sr^{2+}]_i$ transient for phasic release is influenced by the higher Sr^{2+} flux but only little by buffering. ***A***, Fiber stimulation-evoked EPSCs were first recorded in the presence of extracellular Ca^{2+} (2 mM, left) and then after switching the bath solution to 2 mM Sr^{2+} (right). ***B***, Transmitter release rates as obtained by EPSC deconvolution in the presence of Ca^{2+} (left, black trace) and Sr^{2+} (right, red trace). The transmitter release rates predicted by the assumed "local" $[Ca^{2+}]_i$ and $[Sr^{2+}]_i$ transients (***C***) are superimposed (blue traces). ***C***, The back-calculated "local" $[Ca^{2+}]_i$ and $[Sr^{2+}]_i$ transients used to drive the 2-sensor model with the Ca^{2+} and Sr^{2+} sensitivities as determined in the uncaging experiments (Figs. 4 and 6; Table 2). Note that a larger local $[Sr^{2+}]_i$ transient is necessary to explain release rate observed in the presence of Sr^{2+}. ***D***, Individual and average values for the back-calculated peak local $[Ca^{2+}]_i$ and $[Sr^{2+}]_i$ transients ($n = 5$ recordings). Note the ~2-fold larger value of local $[Sr^{2+}]_i$ compared with local $[Ca^{2+}]_i$ ($p < 0.001$). ***$p < 0.001$. ***E***, Traces of local Ca^{2+} and Sr^{2+} concentration as modeled by an M-Cell-based model of Ca^{2+} and Sr^{2+} entry and diffusion (see Materials and Methods). Inset, Spatial arrangement of the model with $n = 8$ Ca^{2+} channels arranged in a circle of 90 µm diameter, surrounding a docked vesicle.

studies with extracellular Sr^{2+}, which concluded that free Sr^{2+} rises to ~1.7-fold higher values than Ca^{2+} and decayed more slowly (Xu-Friedman and Regehr, 1999). However, an ~1.7- to 2-fold increase in free Sr^{2+} compared with Ca^{2+} is expected by only considering the increased Sr^{2+} ion flux through open channels, which we found to be ~1.8-fold for presynaptic Ca^{2+} channels, in good agreement with previous work in cell cultures (Hagiwara and Ohmori, 1982). Because, in addition, the cellular buffering capacity is fivefold lower for Sr^{2+} than for Ca^{2+} (Fig. 7), we expect an overall 10-fold higher spatially averaged Sr^{2+} signal compared with Ca^{2+}. This large factor was borne out in independent imaging experiments with low-affinity indicators (Fig. 8). Finally, we also show that the decay of Sr^{2+} is not strongly prolonged compared with Ca^{2+}, at least in conditions of low exogenously added buffers (Figs. 7 and 8). The latter observation was explained by a near-perfect match of the lower Sr^{2+} extrusion rate γ and by the lower Sr^{2+} buffering capacity κ_S (Fig. 7*F*,*G*).

Endogenous Ca^{2+} buffer(s) limit the rise of spatially averaged $[Ca^{2+}]_i$ following Ca^{2+} influx and the dissipation of Ca^{2+} gradients; the buffer capacity κ_S is defined by the ratio of bound over free Ca^{2+} ions (Neher and Augustine, 1992; Neher, 1998). We found a κ_S value for Ca^{2+} of ~45, in good agreement with a previous study (Helmchen et al., 1997). This value implies that only ~2.5% of all Ca^{2+} ions remain free after equilibration with the buffer. This Ca^{2+} buffering system is largely represented by immobile buffers because whole-cell recording with patch pipettes does not lead to a major loss of buffer capacity (Zhou and Neher, 1993; Müller et al., 2007). The lower buffering capacity for Sr^{2+} ($\kappa_S \sim 8$), corresponds to ~12% of all Sr^{2+} ions remaining free. The ~5-fold lower buffer capacity for Sr^{2+} compared with Ca^{2+} suggests that the Sr^{2+} binding affinity at the endogenous fixed buffer is lower by a similar factor since κ_S can be approximated as $\kappa_S = [S]/K_d$, with [S], concentration of buffer, and K_d, its dissociation constant for the divalent ion (Neher, 1998).

Although the lower affinity of Sr^{2+} at the endogenous fixed buffer caused a drastically larger spatially averaged $[Sr^{2+}]_i$ signal, this mechanism was less relevant for the local Ca^{2+} and Sr^{2+} concentrations that drive phasic release (Fig. 9). Back-calculating the local Ca^{2+} and Sr^{2+} signals for phasic release as well as random walk simulations predicted an only 2.1- to 2.4-fold increase in microdomain Sr^{2+} compared with Ca^{2+} (Fig. 9). This factor can be largely accounted for by the increased flux of Sr^{2+} through Ca^{2+} channels (Fig. 3). This suggests that the endogenous fixed buffer does not strongly contribute to buffering the microdomain divalent ion signal, probably because immobile buffers are rapidly saturated (Roberts, 1994; Naraghi and Neher, 1997). Thus, our study also suggests a divergent action of the endogenous fixed buffer in the control of microdomain versus spatially averaged Ca^{2+} concentration.

It has long been postulated that two separate release sensors mediate fast and asynchronous release, based on the phenotypes of Syt1 KO mice (Geppert et al., 1994), and based on observations with Ca^{2+} and Sr^{2+} (Goda and Stevens, 1994). Similarly, work at the calyx of Held synapse has shown that, in Syt2 KO mice, a release component with low cooperativity remains (Fig. 5) (Sun et al., 2007; Kochubey and Schneggenburger, 2011). We have

therefore used the 2-sensor model (Sun et al., 2007) to fit the Ca^{2+} and Sr^{2+} data, with the modifications that only a single binding site was assumed for the slow sensor (Fig. 5) and that "clamping" of the slow sensor was provided for in the presence of Syt2 (Kochubey and Schneggenburger, 2011) (for details, see Methods and Materials).

Using the refined 2-sensor model fitted to both the Ca^{2+} and the Sr^{2+} uncaging data, we can predict the contribution of the fast and the slow sensors over a wide range of Ca^{2+} and Sr^{2+} concentrations (Fig. 6*C*). Below 0.6 μM $[Ca^{2+}]_i$ and below 3 μM $[Sr^{2+}]_i$, the model predicts that >50% of release, is triggered by the slow sensor; above these concentrations, the fast sensor takes over, as is also apparent by the steep slope values above these concentrations (Fig. 6*B*). Given the measured values of late release rates of ~15 and 150 Hz in the presence of Ca^{2+} and Sr^{2+}, respectively (Fig. 2), which correspond to free $[Ca^{2+}]_i$ and $[Sr^{2+}]_i$ values of ~0.5 and 5 μM, we can see that the late release in the presence of Sr^{2+} falls into a steeper part of the dose–response curve than late release with Ca^{2+} (Fig. 6*B*, red and black dashed lines, respectively). This indicates that reduced Sr^{2+} buffering results in a larger activation of the fast sensor despite the lower sensitivity of the latter for Sr^{2+} as compared to Ca^{2+}. Thus, the activation of fast and slow sensors is more complex than initially thought (Goda and Stevens, 1994), and slow release in the presence of Sr^{2+} can be carried following the activation of the fast, Syt2-like sensor.

These conclusions from detailed fitting of the Ca^{2+} and Sr^{2+} sensitivities of release at the calyx synapse are relevant to other CNS synapses. A steep phase of release has also been observed in Ca^{2+} uncaging experiments at cerebellar inhibitory synapses (Sakaba, 2008) and at hippocampal autaptic synapses (Burgalossi et al., 2010). In addition, the latter study has shown that Syt1 KO leads to a more shallow Ca^{2+}-dependency of release, again demonstrating the persistence of a more linear release sensor in the absence of the main Ca^{2+} sensor, Syt1/2. Some brain synapses, such as GABAergic synapses made by specific interneuron types, are distinguished by slow release kinetics and large asynchronous release (Hefft and Jonas, 2005; Best and Regehr, 2009; Daw et al., 2009). These synapses might both have active zone architectures with longer coupling distances between Ca^{2+} channels and vesicles implying a larger relative importance of global Ca^{2+} signaling; they might also have different mechanisms of intrinsic Ca^{2+} sensing and less clamping of a secondary Ca^{2+} sensor. Future work could investigate the molecular mechanisms that lead to the specification of fast and slow release kinetics at defined types of synapses.

References

Angleson JK, Betz WJ (2001) Intraterminal Ca^{2+} and spontaneous transmitter release at the frog neuromuscular junction. J Neurophysiol 85:287–294. Medline

Best AR, Regehr WG (2009) Inhibitory regulation of electrically coupled neurons in the inferior olive is mediated by asynchronous release of GABA. Neuron 62:555–565. CrossRef Medline

Bollmann JH, Sakmann B, Borst JG (2000) Calcium sensitivity of glutamate release in a calyx-type terminal. Science 289:953–957. CrossRef Medline

Borst JG, Sakmann B (1998) Calcium current during a single action potential in a large presynaptic terminal of the rat brainstem. J Physiol 506:143–157. CrossRef Medline

Burgalossi A, Jung S, Meyer G, Jockusch WJ, Jahn O, Taschenberger H, O'Connor VM, Nishiki T, Takahashi M, Brose N, Rhee JS (2010) SNARE protein recycling by αSNAP and βSNAP supports synaptic vesicle priming. Neuron 68:473–487. CrossRef Medline

Clements JD, Bekkers JM (1997) Detection of spontaneous synaptic events with an optimally scaled template. Biophys J 73:220–229. CrossRef Medline

Daw MI, Tricoire L, Erdelyi F, Szabo G, McBain CJ (2009) Asynchronous transmitter release from cholecystokinin-containing inhibitory interneurons is widespread and target-cell independent. J Neurosci 29:11112–11122. CrossRef Medline

Delaney KR, Tank DW (1994) A quantitative measurement of the dependence of short-term synaptic enhancement on presynaptic residual calcium. J Neurosci 14:5885–5902. Medline

Dodge FA Jr, Rahamimoff R (1967) Co-operative action of calcium ions in transmitter release at the neuromuscular junction. J Physiol 193:419–432. Medline

Ellis-Davies GC (2003) Development and application of caged Calcium. Methods Enzymol 360:226–238. CrossRef Medline

Fernández-Chacón R, Königstorfer A, Gerber SH, García J, Matos MF, Stevens CF, Brose N, Rizo J, Rosenmund C, Südhof TC (2001) Synaptotagmin I functions as a calcium regulator of release probability. Nature 410:41–49. CrossRef Medline

Geppert M, Goda Y, Hammer RE, Li C, Rosahl TW, Stevens CF, Südhof TC (1994) Synaptotagmin I: a major Ca^{2+} sensor for transmitter release at a central synapse. Cell 79:717–727. CrossRef Medline

Goda Y, Stevens CF (1994) Two components of transmitter release at a central synapse. Proc Natl Acad Sci U S A 91:12942–12946. CrossRef Medline

Grynkiewicz G, Poenie M, Tsien RY (1985) A new generation of Ca^{2+} indicators with greatly improved fluorescence properties. J Biol Chem 260:3440–3450. Medline

Hagiwara S, Ohmori H (1982) Studies of calcium channels in rat clonal pituitary cells with patch electrode voltage clamp. J Physiol 331:231–252. Medline

Hefft S, Jonas P (2005) Asynchronous GABA release generates long-lasting inhibition at a hippocampal interneuron-principal neuron synapse. Nat Neurosci 8:1319–1328. CrossRef Medline

Helmchen F, Borst JG, Sakmann B (1997) Calcium dynamics associated with a single action potential in a CNS presynaptic terminal. Biophys J 72:1458–1471. CrossRef Medline

Kerr RA, Bartol TM, Kaminsky B, Dittrich M, Chang JC, Baden SB, Sejnowski TJ, Stiles JR (2008) Fast Monte Carlo simulation methods for biological reaction-diffusion systems in solution and on surfaces. SIAM J Sci Comput 30:3126–3173. CrossRef Medline

Kirischuk S, Grantyn R (2003) Intraterminal Ca^{2+} concentration and asynchronous transmitter release at single GABAergic boutons in rat collicular cultures. J Physiol 548:753–764. CrossRef Medline

Kishimoto T, Liu TT, Ninomiya Y, Takagi H, Yoshioka T, Ellis-Davies GC, Miyashita Y, Kasai H (2001) Ion selectivities of the Ca^{2+} sensors for exocytosis in rat phaeochromocytoma cells. J Physiol 533:627–637. CrossRef Medline

Kochubey O, Schneggenburger R (2011) Synaptotagmin increases the dynamic range of synapses by driving Ca^{2+}-evoked release and by clamping a near-linear remaining Ca^{2+} sensor. Neuron 69:736–748. CrossRef Medline

Kochubey O, Han Y, Schneggenburger R (2009) Developmental regulation of the intracellular Ca^{2+} sensitivity of vesicle fusion and Ca^{2+}-secretion coupling at the rat calyx of Held. J Physiol 587:3009–3023. CrossRef Medline

Lou X, Scheuss V, Schneggenburger R (2005) Allosteric modulation of the presynaptic Ca^{2+} sensor for vesicle fusion. Nature 435:497–501. CrossRef Medline

Mackler JM, Drummond JA, Loewen CA, Robinson IM, Reist NE (2002) The C2B Ca^{2+}-binding motif of synaptotagmin is required for synaptic transmission *in vivo*. Nature 418:340–344. CrossRef Medline

Martell AE, Smith RM (1974) Critical stability constants, Vol 1. New York: Plenum.

Meinrenken C, Borst JG, Sakmann B (2002) Calcium secretion coupling at calyx of Held governed by nonuniform channel-vesicle topography. J Neurosci 22:1648–1667. Medline

Miledi R (1966) Strontium as a substitute for calcium in the process of transmitter release at the neuromuscular junction. Nature 212:1233–1234. CrossRef Medline

Müller M, Felmy F, Schwaller B, Schneggenburger R (2007) Parvalbumin is a mobile presynaptic Ca^{2+} buffer in the calyx of Held that accelerates the

decay of Ca^{2+} and short-term facilitation. J Neurosci 27:2261–2271. CrossRef Medline

Naraghi M, Neher E (1997) Linearized buffered Ca^{2+} diffusion in microdomains and its implications for calculation of [Ca^{2+}] at the mouth of a calcium channel. J Neurosci 17:6961–6973. Medline

Neher E (1998) Usefulness and limitations of linear approximations to the understanding of Ca^{++} signals. Cell Calcium 24:345–357. CrossRef Medline

Neher E, Augustine GJ (1992) Calcium gradients and buffers in bovine chromaffin cells. J Physiol 450:273–301. Medline

Neher E, Sakaba T (2001) Combining deconvolution and noise analysis for the estimation of transmitter release rates at the calyx of Held. J Neurosci 21:444–461. Medline

Nishiki T, Augustine GJ (2004) Dual roles of the C2B domain of synaptotagmin I in synchronizing Ca^{2+}-dependent neurotransmitter release. J Neurosci 24:8542–8550. CrossRef Medline

Pang ZP, Melicoff E, Padgett D, Liu Y, Teich AF, Dickey BF, Lin W, Adachi R, Südhof TC (2006) Synaptotagmin-2 is essential for survival and contributes to Ca^{2+} triggering of neurotransmitter release in central and neuromuscular synapses. J Neurosci 26:13493–13504. CrossRef Medline

Ravin R, Spira ME, Parnas H, Parnas I (1997) Simultaneous measurement of intracellular Ca^{2+} and asynchronous transmitter release from the same crayfish bouton. J Physiol 501:251–262. Medline

Roberts WM (1994) Localization of calcium signals by a mobile calcium buffer in frog saccular hair cells. J Neurosci 14:3246–3262. Medline

Rumpel E, Behrends JC (1999) Sr^{2+}-dependent asynchronous evoked transmission at rat striatal inhibitory synapses *in vitro*. J Physiol 514:447–458. CrossRef Medline

Sakaba T (2008) Two Ca^{2+}-dependent steps controlling synaptic vesicle fusion and replenishment at the cerebellar basket cell terminal. Neuron 57:406–419. CrossRef Medline

Sakaba T, Neher E (2001) Calmodulin mediates rapid recruitment of fast-releasing synaptic vesicles at a calyx-type synapse. Neuron 32:1119–1131. CrossRef Medline

Schneggenburger R, Neher E (2000) Intracellular calcium dependence of transmitter release rates at a fast central synapse. Nature 406:889–893. CrossRef Medline

Schneggenburger R, Meyer AC, Neher E (1999) Released fraction and total size of a pool of immediately available transmitter quanta at a calyx synapse. Neuron 23:399–409. CrossRef Medline

Shin OH, Rhee JS, Tang J, Sugita S, Rosenmund C, Südhof TC (2003) Sr^{2+} binding to the Ca^{2+} binding site of the synaptotagmin 1 C2B domain triggers fast exocytosis without stimulating SNARE interactions. Neuron 37:99–108. CrossRef Medline

Sun J, Pang ZP, Qin D, Fahim AT, Adachi R, Südhof TC (2007) A dual-Ca^{2+}-sensor model for neurotransmitter release in a central synapse. Nature 450:676–682. CrossRef Medline

von Gersdorff H, Schneggenburger R, Weis S, Neher E (1997) Presynaptic depression at a calyx synapse: the small contribution of metabotropic glutamate receptors. J Neurosci 17:8137–8146. Medline

Wang LY, Kaczmarek LK (1998) High-frequency firing helps replenish the readily releasable pool of synaptic vesicles. Nature 394:384–388. CrossRef Medline

Wang LY, Fedchyshyn MJ, Yang YM (2009) Action potential evoked transmitter release in central synapses: insights from the developing calyx of Held. Mol Brain 2:36–46. CrossRef Medline

Wilson JE, Chin A (1991) Chelation of divalent cations by ATP, studied by titration calorimetry. Anal Biochem 193:16–19. CrossRef Medline

Wölfel M, Lou X, Schneggenburger R (2007) A mechanism intrinsic to the vesicle fusion machinery determines fast and slow transmitter release at a large CNS synapse. J Neurosci 27:3198–3210. CrossRef Medline

Xu-Friedman MA, Regehr WG (1999) Presynaptic strontium dynamics and synaptic transmission. Biophys J 76:2029–2042. CrossRef Medline

Xu-Friedman MA, Regehr WG (2000) Probing fundamental aspects of synaptic transmission with strontium. J Neurosci 20:4414–4422. Medline

Yoshihara M, Littleton JT (2002) Synaptotagmin I functions as a calcium sensor to synchronize neurotransmitter release. Neuron 36:897–908. CrossRef Medline

Zhou Z, Neher E (1993) Mobile and immobile calcium buffers in bovine adrenal chromaffin cells. J Physiol 469:245–273. Medline